Icarus **153**, 162–179 (2001)
doi:10.1006/icar.2001.6678, available online at http://www.idealibrary.com on IDEAL®

Ethane Production and Release in Comet C/1995 O1 Hale–Bopp

Neil Dello Russo

Department of Physics, Catholic University of America, Washington, D.C. 20064; and Laboratory for Extraterrestrial Physics, NASA Goddard Space Flight Center Code 690.2, Greenbelt, Maryland 20771
E-mail: ysndr@lepvax.gsfc.nasa.gov

Michael J. Mumma

Laboratory for Extraterrestrial Physics, NASA Goddard Space Flight Center Code 690, Greenbelt, Maryland 20771

Michael A. DiSanti

Department of Physics, Catholic University of America, Washington, D.C.; and Laboratory for Extraterrestrial Physics, NASA Goddard Space Flight Center Code 690.2, Greenbelt, Maryland 20771

Karen Magee-Sauer

Department of Chemistry and Physics, Rowan University, Glassboro, New Jersey 08028

and

Robert Novak

Department of Physics, Iona College, New Rochelle, New York 10801

Received December 15, 2000; revised April 25, 2001

Ethane (C_2H_6) was detected in Comet C/1995 O1 Hale–Bopp on 13 dates between UT 1996 September 20.3 ($R_h = 3.01$ AU pre-perihelion) and 1997 September 25.7 ($R_h = 2.83$ AU post-perihelion) using high-resolution infrared spectroscopy. Production rates and rotational temperatures were measured, and the derived heliocentric dependence for ethane production was $Q = (5.52 \pm 0.20) \times 10^{28}\ [R_h^{(-2.43 \pm 0.13)}]$ molecules s^{-1}. The spatial distribution of C_2H_6 molecules in the coma was consistent with all ethane being released directly from the nucleus, although the possibility that a small fraction was released as a distributed source cannot be excluded. When our derived production rates for ethane, water, and acetylene (C_2H_2) are compared, we obtain an average relative abundance of $C_2H_6/H_2O = (6.23 \pm 0.42) \times 10^{-3}$, and $C_2H_6/C_2H_2 = 2.4 \pm 0.7$. The high ethane abundance relative to acetylene in Hale–Bopp suggests its ices were altered by radiation processing and/or hydrogen-atom addition reactions on the surfaces of ice-mantled grains in the natal cloud. These results are not consistent with ices in Hale–Bopp originating in a thermally or chemically equilibrated region of the solar nebula.

Key Words: **comets, Hale–Bopp; composition; infrared observations; ethane.**

1. INTRODUCTION

Comets are volatile-rich, relatively unaltered remnants from the birth of the Solar System, whose chemical compositions may reflect conditions in their formative regions. Conditions were likely quite diverse in the early solar nebula, since temperatures and radiation doses should have varied significantly with distance from the young Sun. Beyond Neptune, the great distance from the Sun and the large amount of intervening nebular material should have offered protection against extensive thermal and radiation processing. Hence, comets formed in the Kuiper belt may contain primarily unmodified interstellar ices. However, ices in the giant planets' region were subjected to more intense radiation doses and to higher temperatures (mid-plane temperatures ranged from ∼150 K near Jupiter to ∼40 K near Neptune). Comets formed there may possess diverse chemistries reflective of their individual processing histories. Knowledge of cometary composition is essential for constraining physical and chemical conditions in the early solar nebula, and it thus forms a central problem in cometary science.

The volatile composition of the nucleus has generally been inferred from the spectral signatures of gases forming the coma.

0019-1035/01$35.00

While dissociation fragments have been studied for nearly one-hundred years, it is often difficult to deduce their parent species. Prior to 1985, CO was detected in two comets at ultraviolet wavelengths (West 1976 VI and Bradfield 1979 X; cf. Feldman 1983); however, CO can also be produced both as a parent and a dissociation fragment. The direct study of other parent volatiles became possible with the detection of HCN (Despois *et al.* 1986, Schloerb *et al.* 1986) and H_2O (Mumma *et al.* 1986) in Comet Halley. Improvements in astronomical capabilities since Comet Halley have permitted detection of an increasing number of species, with more than two dozen parent volatiles being identified in the exceptionally bright Comet Hale–Bopp (cf. Crovisier 1998).

Close spacecraft encounters with Comet Halley also greatly increased our knowledge of the volatile content of the coma and the nucleus. The neutral gas mass spectrometer (NMS) aboard *Giotto* provided measurements of several native species, including a recent retrospective identification of ethane (Eberhardt *et al.* 1987, Eberhardt 1999). The IKS infrared spectrometer on the *Vega 1* spacecraft achieved detections of H_2O, CO_2, H_2CO, and possibly CO (Combes *et al.* 1986, 1988; Mumma and Reuter 1989). IKS also detected a spectral signature in the region 3.2–3.6 μm attributed primarily to C–H stretching vibrations in one or more organic compounds (Combes *et al.* 1988). The PIA/PUMA dust composition analyzer discovered a population of dust particles composed of an organic material containing carbon, hydrogen, oxygen, and nitrogen (CHON grains; Kissel *et al.* 1986, Jessberger *et al.* 1988), leading Greenberg and Hage (1990) to suggest fluffy organic grains as a source for the *X*–CH emission feature. However, increasing evidence suggests that this feature is composed primarily of infrared fluorescence from volatile species (e.g., CH_3OH, C_2H_6, CH_4, OH) (Hoban *et al.* 1991; Reuter 1992; Bockelée-Morvan *et al.* 1995; Mumma *et al.* 1996, 2001a).

The detection of methanol (CH_3OH) in Comet C/1989 X1 Austin (Hoban *et al.* 1991, Bockelée-Morvan *et al.* 1991) and the subsequent modeling of its ν_2, ν_3, and ν_9 bands (Reuter 1992) showed that methanol could contribute some (but not all) of the integrated flux measured in the *X*–CH feature. Presumably, emissions due to gas phase fluorescence from other organic species were also present, but detecting, isolating, and quantifying other contributing species was problematic at the low spectral resolution then available. Observations of other comets supported the view that gas phase fluorescence was primarily responsible for the bulk of the *X*–CH emission, but the relative contribution of thermal emission from organic grains remained an open question (DiSanti *et al.* 1995, Bockelée-Morvan *et al.* 1995 and references therein).

With recent instrumental advances, ground-based studies can now be done with greater sensitivity and higher spectral resolution. High-resolution ($\lambda/\Delta\lambda > 10^4$) infrared spectroscopy enables individual ro-vibrational lines to be resolved and differentiated from telluric absorptions, other molecular emissions, and the continuum, making accessible species that are not observable with low resolution. The discovery in Comet Hyakutake of methane (CH_4), ethane (C_2H_6), and acetylene (C_2H_2) (Mumma *et al.* 1996, Brooke *et al.* 1996) established the importance of these symmetric hydrocarbons in comets. The spectra showed that CH_4 and C_2H_6 can contribute to the *X*–CH feature (along with CH_3OH and possibly organic grains) and are thus key to interpreting low-resolution spectral data. Moreover, their abundances provide crucial information on the link between interstellar and cometary ices (cf. Mumma 1997).

The apparition of the bright Comet C/1995 O1 Hale–Bopp provided an opportunity to track cometary activity as a function of heliocentric distance, and to study the release of volatile species. Here, we report a comprehensive study of ethane release in Comet Hale–Bopp, within 3.01 AU of the Sun. The high spectral resolution of our data allows the determination of C_2H_6 rotational temperatures and production rates through the detection of multiple *Q*-branches in the ν_7 band near 3.35 μm. The high spatial resolution of our measurements helps reveal the connection between the distribution of C_2H_6 vapor in the coma and its presence as a native ice in the nucleus. Our analysis shows that C_2H_6 was present in Hale–Bopp with a high abundance relative to C_2H_2 and CH_4, and that most (if not all) of it was released directly from ices in the nucleus on the dates studied. We also comment on the nondetection of ethylene (C_2H_4) and propane (C_3H_8) in Hale–Bopp.

2. OBSERVATIONS AND DATA ANALYSIS

Multiple *Q*-branches from the ν_7 band of C_2H_6 were detected on 13 dates between UT 1996 Sep. 20.3 ($R_h = 3.01$ AU pre-perihelion), and UT 1997 Sep. 25.7 ($R_h = 2.83$ AU post-perihelion) in Comet Hale–Bopp (Table I; Figs. 1, 2, 3). Ethane was searched for on UT 1996 June 12.6 ($R_h = 4.12$ AU), and an upper limit was determined. We used the cryogenic echelle spectrometer (CSHELL) at the NASA Infrared Telescope Facility on Mauna Kea, Hawaii (Greene *et al.* 1993). CSHELL has a 256×256 pixel InSb array detector with a pixel size of 0.2 arcsec, and provides spatial coverage along the 30-arcsec-long slit, which we oriented east–west. A 1-arcsec-wide slit was used for our comet observations leading to a spectral resolving power $\lambda/\Delta\lambda \sim 2 \times 10^4$. At each grating setting, cometary data were acquired using a sequence of four scans (*ABBA*, where $A =$ source and $B =$ sky), with an integration time of two minutes on source per scan sequence. Sky spectra were obtained by nodding the telescope 2 arcmin from the source, providing sky cancellation via pixel-by-pixel subtraction. Flat-fields and dark frames were obtained immediately following each scan sequence. For each grating setting, spectra of infrared standard stars were obtained through a 4-arcsec-wide slit for absolute flux calibration of the comet spectra.

Although prodigiously bright, Comet Hale–Bopp was generally available only during daylight hours when variations in atmospheric seeing and the inability to track the comet with the telescope's autoguider significantly decreased our observing

TABLE I
CSHELL C_2H_6 Observations in Comet C/1995 O1 Hale–Bopp

UT date	R_h (AU)	Δ (AU)	$\dot{\Delta}$ (km s^{-1})	PA[a]	β[b]	C_2H_6 Q-branches targeted[c]
1996 Jun 12.6[d]	4.11	3.19	−31.0	246	7	$^{R}Q_0$, $^{P}Q_1$
1996 Sep 20.3	3.01	2.93	+9.7	91	19	$^{R}Q_0$, $^{P}Q_1$
1996 Dec 11.1	2.02	2.83	−18.0	31	13	$^{R}Q_0$, $^{P}Q_1$
1997 Jan 21.8	1.49	2.20	−32.6	336	22	$^{R}Q_0$, $^{P}Q_1$
1997 Feb 24.0	1.11	1.57	−29.1	327	39	$^{R}Q_0$, $^{R}Q_1$, $^{R}Q_3$, $^{R}Q_4$ $^{P}Q_1$, $^{P}Q_3$, $^{P}Q_4$
1997 Apr 6.2	0.92	1.40	+18.4	36	46	$^{R}Q_0$, $^{P}Q_1$
1997 Apr 8.1	0.92	1.42	+20.1	40	45	$^{R}Q_0$, $^{R}Q_3$, $^{R}Q_4$, $^{P}Q_1$
1997 Apr 9.0	0.93	1.43	+20.9	42	44	$^{R}Q_0$, $^{R}Q_1$, $^{R}Q_2$, $^{R}Q_3$, $^{R}Q_4$ $^{P}Q_1$, $^{P}Q_2$, $^{P}Q_3$
1997 Apr 10.2	0.93	1.44	+21.9	44	43	$^{R}Q_0$, $^{P}Q_1$
1997 Apr 30.0	1.05	1.75	+29.7	75	31	$^{R}Q_0$, $^{R}Q_1$, $^{R}Q_2$, $^{R}Q_3$, $^{R}Q_4$ $^{P}Q_1$, $^{P}Q_2$, $^{P}Q_3$
1997 May 1.2	1.06	1.77	+29.7	76	30	$^{R}Q_0$, $^{R}Q_1$, $^{R}Q_2$, $^{R}Q_3$ $^{R}Q_4$, $^{P}Q_1$
1997 Aug 7.9	2.24	2.91	+8.7	220	17	$^{R}Q_0$, $^{P}Q_1$
1997 Aug 8.8	2.25	2.91	+8.6	221	17	$^{R}Q_0$, $^{P}Q_1$
1997 Sep 25.7	2.83	3.09	+5.7	253	19	$^{R}Q_0$, $^{P}Q_1$

[a] Position angle (degrees) of the extended radius vector in the anti-solar direction projected onto the sky plane and measured eastward from north.

[b] Sun–comet–Earth angle (degrees). On all dates spanning our Hale–Bopp observations, β was slightly acute; thus the anti-solar direction was largely away from the observer.

[c] $^{R}Q_3$ Q-branch is blended with methanol and OH emission, so it was not used for quantitative analysis.

[d] C_2H_6 was searched for but not detected.

efficiency. Tracking rates were checked and updated by taking images of the comet through a circular variable filter at 3.5 or 2.2 μm before and after each sequence of scans. Defocusing can occur if sunlight strikes the telescope structure, so focus was also checked and updated regularly using a star close to the comet. These factors (and perhaps other unrecognized ones) influenced not only the observing efficiency, but also the quality of the data inside the region affected by "nonideal" observing conditions (Dello Russo *et al.* 2000). The quality of observing conditions can be estimated and monitored by periodically obtaining a point spread function (PSF) of a star. For our observations, the full-width at half-maximum (FWHM) of a stellar PSF was typically ~1–2 arcsec and it generally varied within a single date.

The data were processed using algorithms specifically tailored to our comet observations. Step-wise application of these has been presented (Dello Russo *et al.* 1998, Magee-Sauer *et al.* 1999, DiSanti *et al.* 2001). Initial processing included flat-fielding, removal of high dark current pixels and cosmic ray hits, and registration of spectral frames such that the spectral dimension falls along a row and the spatial dimension is orthogonal to this (Fig. 1A). Spectra can then be extracted over any desired spatial extent and position along the slit (Fig. 1B). Atmospheric models were obtained using the Spectrum Synthesis Program (SSP) (Kunde and Maguire 1974), which accesses the HITRAN-1992 Molecular Data Base (Rothman *et al.* 1992). SSP models were used to assign wavelength scales to the extracted spectra, and to establish absolute column burdens for each significant absorbing species in the terrestrial atmosphere. The fully resolved model was binned to the instrumental sampling interval, convolved to the resolution of the comet spectrum, and normalized to the cometary continuum (Fig. 1B). Volatile emission features were separated from the continuum by subtracting the normalized atmospheric model from the comet spectrum row by row, yielding the net cometary molecular emissions still convolved with the atmospheric transmittance function (Figs. 1C, 1D, 2). The true Q-branch flux incident at the top of the terrestrial atmosphere was obtained from the observed flux by correcting for the monochromatic transmittance obtained from the fully resolved SSP model at the Doppler-shifted Q-branch position.

3. DETERMINATION OF *g*-FACTORS AND ROTATIONAL TEMPERATURES

Production rates may be derived from measured Q-branch fluxes if the fluorescence efficiencies (g-factors) and their dependence on temperature are known. For the C_2H_6 ν_7 band, each Q-branch consists of temperature-dependent lines for $J \geq K$ from two torsional tunneling sublevels. The relative intensities of individual J-lines within a Q-branch could provide a very sensitive measure of the rotational temperature; however, these lines have been fully resolved only in the laboratory using sub-Doppler molecular-beam spectroscopy (Pine and Stone 1996). In order to derive Q-branch g-factors, the population distribution of rotational levels in the ground vibrational state must be known. The rotational temperature in the excited state is determined from the relative emission intensities of the observed C_2H_6 Q-branches, and we assume that the rotational temperature in the ground and excited vibrational states are equal. From this assumption, the population distribution of rotational levels in the ground vibrational state were determined, and g-factors for individual Q-branches (Table II) were calculated using a simple temperature-dependent fluorescence model (see Appendix for details).

In our CSHELL comet spectra, the individual J-lines are not resolved, so we observe only the composite of all J-lines contributing to a given Q-branch. Relative Q-branch intensities are not a very sensitive indicator of rotational temperature since each Q-branch reflects a range of energies rather than a discrete value. As a result our derived rotational temperatures are not well constrained (Table IV). On dates where only the

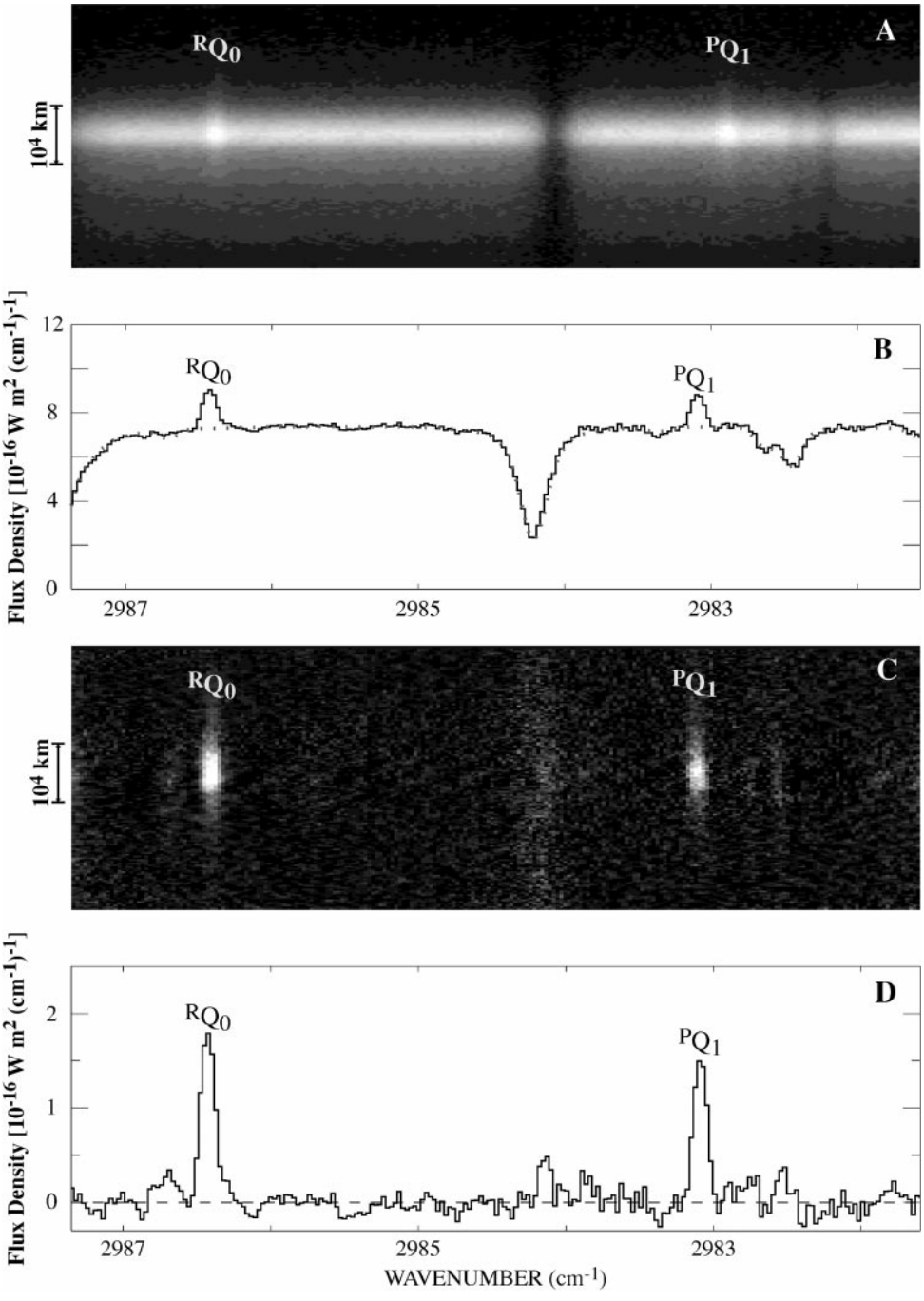

FIG. 1. Detection of C_2H_6 in Comet Hale–Bopp on UT 1997 May 1.2. (A) On-chip spatial–spectral image showing molecular emissions and the dust continuum. The spatial dimension is along columns and the spectral dimension is along rows. The spatial extent of the image is ∼30 arcsec on the sky, with a spatial scale displayed on the left. East is at the top. (B) Flux-calibrated cometary spectral extract (solid curve). The displayed spectral extract has a spatial extent of 1 arcsec (5 rows) and is centered on the nucleus. Ethane $^{R}Q_0$ and $^{P}Q_1$ emissions are clearly seen above the optimized atmospheric model spectrum (dotted curve). (C) The residual spectral image shown in (A) after removal of the dust continuum via row-by-row scaled subtraction of the atmospheric model. (D) Flux-calibrated residual spectral extract. The displayed residual spectrum has a spatial extent of 1 arcsec (5 rows) and is centered on the nucleus.

$^{R}Q_0$ and $^{P}Q_1$ Q-branches were detected, a rotational temperature could not be derived, so a reasonable rotational temperature was adopted. On April 6.2 and 10.2, a rotational temperature of 128 K was adopted based on a weighted average of derived C_2H_6 rotational temperatures on April 8.1 and 9.0 (Table IV). On dates when $R_h \geq 1.48$ AU, rotational temperatures were adopted based on values derived in Biver *et al.* (1999) for CH_3OH and CO at similar heliocentric distances. The

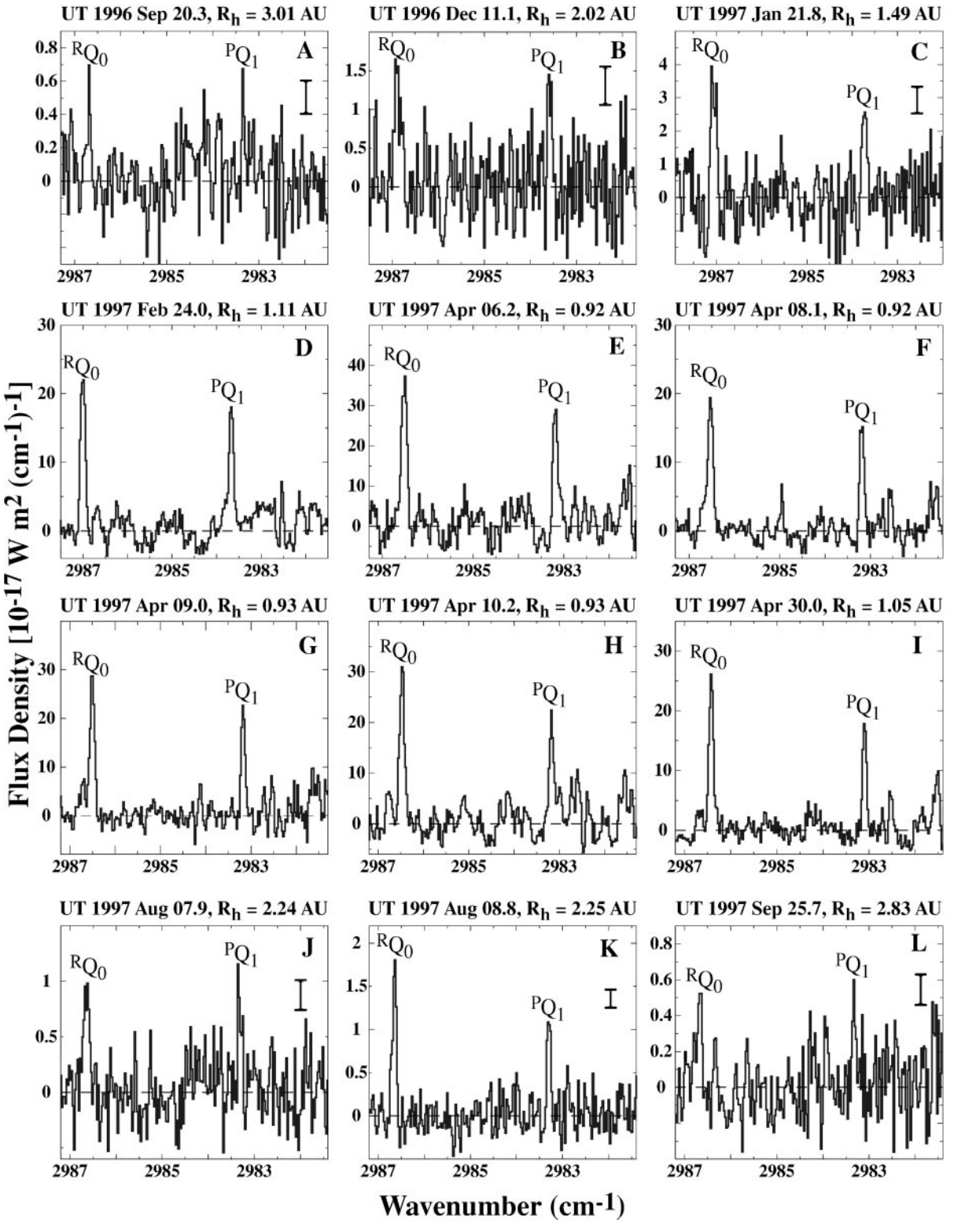

FIG. 2. Detection of the C_2H_6 $^RQ_0$ and $^PQ_1$ Q-branches in Hale–Bopp on 12 dates. Flux-calibrated residual spectra are obtained by subtracting normalized atmospheric transmittance spectra from cometary spectra containing both continuum and molecular emissions. The displayed spectra were extracted over spatial extents of 1 arcsec (5 rows) centered on the nucleus. (A) UT 1996 Sep. 20.3. (B) UT 1996 Dec. 11.1. (C) UT 1997 Jan. 21.8. (D) UT 1997 Feb. 24.0. (E) UT 1997 Apr. 6.2. (F) UT 1997 Apr. 8.1. (G) UT 1997 Apr. 9.0. (H) UT 1997 Apr. 10.2. (I) UT 1997 Apr. 30.0. (J) UT 1997 Aug. 7.9. (K) UT 1997 Aug. 8.8. (L) UT 1997 Sep. 25.7. (UT 1997 May 1.2 is shown in Fig. 1D). On dates when $R_h \geq 1.48$ AU, the uncertainty is dominated by photon noise, so 1σ error bars are shown on the right side of the figure. On dates when $R_h < 1.48$ AU, the uncertainty is dominated by deviations in the synthetic atmospheric model fit, and instrumental effects.

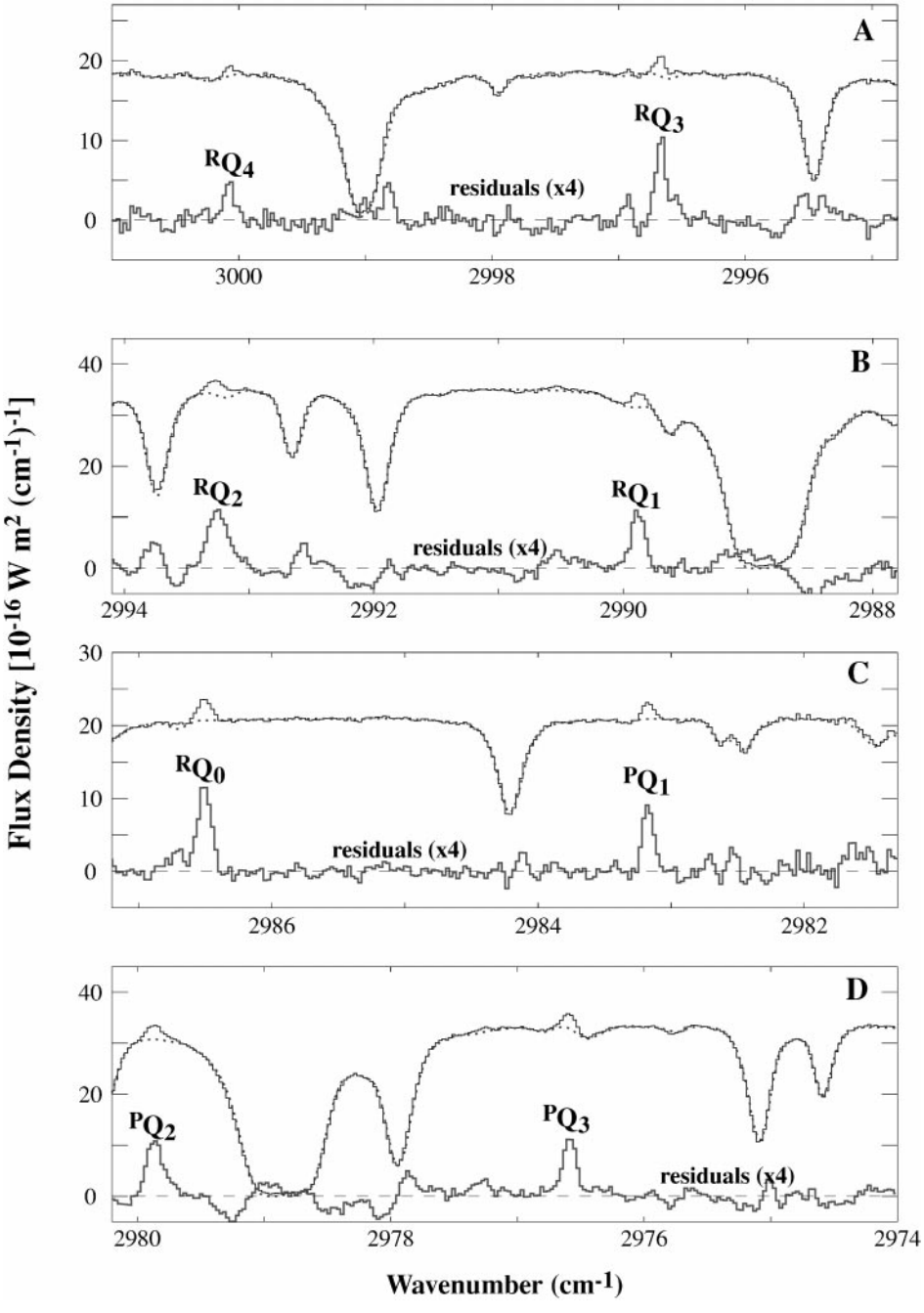

FIG. 3. Flux-calibrated spectra of Comet Hale–Bopp representing four grating settings that together show the detection of eight C_2H_6 ν_7 Q-branches on UT 1997 Apr. 9.0. Each panel shows cometary continuum and molecular emission (solid curve), a normalized atmospheric transmittance spectrum (dotted curve), and their difference (residual spectrum multiplied by 4): (A) $^RQ_4$ and $^RQ_3$, (B) $^RQ_2$ and $^RQ_1$, (C) $^RQ_0$ and $^PQ_1$, (D) $^PQ_2$ and $^PQ_3$. The displayed spectral extracts have a spatial extent of 1 arcsec (5 rows) and are centered on the nucleus (because these spectra are nucleus-centered extracts, differences in flux densities between them are primarily due to variations in seeing and pointing).

sensitivity of production rates to derived rotational temperature is modest: A difference of 30 K in rotational temperature changes the production rate derived from an individual Q-branch by $<20\%$ (Table II). Production rates derived from each Q-branch are given in Table III and the results for each date are summarized in Table IV.

4. THE SPATIAL DISTRIBUTION OF ETHANE IN COMET HALE–BOPP

Measured volatile abundances in the coma do not necessarily correspond to the composition of ices in the comet nucleus, since coma abundances alone do not reveal how volatiles arrived

TABLE II
Ethane ν_7 Q-branch Positions and g-Factors

ν_7 Q-branch	Rest frequency (cm^{-1})[a]	g-factors (10^{-5} s^{-1})[b]
$^{P}Q_4$	2973.47	1.40 (70 K)
		1.43 (100 K)
		1.39 (130 K)
$^{P}Q_3$	2976.77	2.19 (70 K)
		2.07 (100 K)
		1.91 (130 K)
$^{P}Q_2$	2980.07	3.08 (70 K)
		2.70 (100 K)
		2.39 (130 K)
$^{P}Q_1$	2983.38	3.40 (70 K)
		2.85 (100 K)
		2.46 (130 K)
$^{R}Q_0$	2986.73	3.77 (70 K)
		3.19 (100 K)
		2.76 (130 K)
$^{R}Q_1$	2990.09	3.04 (70 K)
		2.73 (100 K)
		2.44 (130 K)
$^{R}Q_2$	2993.48	2.12 (70 K)
		2.05 (100 K)
		1.92 (130 K)
$^{R}Q_3$	2996.87	1.68 (70 K)
		1.79 (100 K)
		1.77 (130 K)
$^{R}Q_4$	3000.28	0.90 (70 K)
		1.12 (100 K)
		1.22 (130 K)

[a] Values taken from Mélen *et al.* (1993).
[b] As a function of temperature for $R_h = 1$ AU (see Appendix).

there. A volatile may sublime directly from ice in the nucleus (native source) or be released in the coma as a distributed source (whether from grains, as a photodissociation product, or by active coma chemistry). Discerning different source contributions in the coma can reveal information on the physical nature and composition of the cometary nucleus. A more complete connection between nuclear ices and coma gases can be established by measuring the spatial distribution (or spatial profile) of a species in the coma.

Neglecting outflow asymmetries, the column density of a volatile (or dust) sublimed directly from the nucleus (with no additional distributed component) should fall off as ρ^{-1}, where ρ is the projected distance from the nucleus. This is valid as long as ρ is small compared to the photodissociation scale length of the species. (The photodissociation lifetime of ethane is $\sim 9 \times 10^4$ s at 1 AU; hence its scale length is $\sim 10^5$ km in Hale–Bopp near perihelion.) The spatial profile for a species with a significant distributed source will be broader, falling off more slowly than ρ^{-1} (e.g., CO, see DiSanti *et al.* 1999, 2001). However, properties of the comet (e.g., jets), observing conditions, and optical depth effects (not important for C_2H_6 in Hale–Bopp) can also affect profile shapes, causing deviations from a ρ^{-1} distribution even for purely native species (Dello Russo *et al.* 2000, DiSanti *et al.* 2001). We have demonstrated that comparison of spatial profiles for volatile species and dust (measured simultaneously) can provide a means for assessing the presence of a significant distributed source. However, such comparisons cannot reliably identify contributions from small distributed sources close to the nucleus (see DiSanti *et al.* (1999, 2001) Dello Russo *et al.* (2000) for detailed discussion).

The spatial resolution afforded by CSHELL allowed the measurement of spatial profiles for C_2H_6 (Fig. 4). In general, asymmetries in spatial profiles are more severe for the dust than for parent volatiles, since outflowing gas is isotropized more effectively by collisions than is dust. Comparison of spatial profiles show that on some dates C_2H_6 and dust outflow seem to track one another (e.g. Fig. 4C), while on other dates they differ significantly (e.g., Fig. 4D). Despite relative differences in outflow of C_2H_6 and dust on some dates, on all dates their spatial profiles each fall off as approximately ρ^{-1} beyond $\sim$1–2 arcsec from the nucleus (the region within $\sim$1–2 arcsec is affected by seeing, Fig. 4). This suggests that most if not all ethane is released directly from the nucleus in Hale–Bopp on all 13 dates, although a small contribution from a distributed source cannot be ruled out. An analysis from independent CSHELL observations on UT March 5 ($R_h \sim 1.03$ AU) is also consistent with C_2H_6 being released directly from ices in the nucleus (Weaver *et al.* 1999a). Spatial profiles for several other volatile species (H_2O, CO, HCN, and OCS) were also obtained at infrared wavelengths in Hale–Bopp. Analyses indicated that H_2O and HCN were primarily released directly from the nucleus, while CO (at $R_h \leq 1.5$ AU) and OCS (at $R_h = 0.95$ AU) had significant distributed source contributions (Dello Russo *et al.* 1998, 2000; DiSanti *et al.* 1999, 2001; Magee-Sauer *et al.* 1999; Weaver *et al.* 1999a). A comparison of H_2O and C_2H_6 spatial profiles also suggests a primarily native source for ethane (Fig. 4B).

5. ETHANE PRODUCTION RATES

The high spatial resolution afforded by CSHELL allows "spherical" production rates for strong emissions to be determined at different positions along the slit. For this purpose, we assume all C_2H_6 is produced at the nucleus and flows outward with spherical symmetry and with uniform velocity. A spherical production rate is determined from the flux contained within a 1×1-arcsec^2 box. When this box is stepped at 1-arcsec intervals along the slit, the sequence of spherical production rates constitutes a Q-curve (Figs. 5A and 5B; also see Dello Russo *et al.* 1998, 2000; Magee-Sauer *et al.* 1999; DiSanti *et al.* 2001).

The production rate (molecules s^{-1}) at a given step is calculated as follows:

$$Q = \frac{4\pi \Delta^2 F_i}{g_i \tau (hc\nu) f(x)}.$$

The photodissociation lifetime τ (s) and Q-branch g-factor g_i (photons s^{-1} molecule^{-1}) are both calculated for $R_h = 1$ AU. Δ is the geocentric distance in meters, $hc\nu$ is the energy (J)

TABLE III
Derived Line Fluxes and Production Rates for ν_7 Ethane Q-Branches in Comet Hale–Bopp

UT date	Infrared flux standard stars[a]	Q-branch[b]	Line flux (10^{-17} Wm^{-2})[d]	Q (C_2H_6) (10^{28} mol s^{-1})[f]
1996 Jun. 12.6	BS 6147 (ϕ Oph)	$^{R}Q_0 + {}^{P}Q_1^c$	$<0.06^e$	$<0.6^g$
1996 Sep. 20.3	BS 1165 (η Tau)	$^{R}Q_0 + {}^{P}Q_1$	0.075 ± 0.017^e	0.29 ± 0.12^g
1996 Dec. 11.1	BS 8551 (35 Peg)	$^{R}Q_0 + {}^{P}Q_1$	0.72 ± 0.11	0.79 ± 0.20
1997 Jan. 21.8	BS 6707 (ν Her)	$^{R}Q_0 + {}^{P}Q_1$	4.18 ± 0.49	2.15 ± 0.47
1997 Feb. 24.0	BS 1165	$^{R}Q_0$	10.25 ± 0.29	4.92 ± 0.26
		$^{R}Q_0$	11.15 ± 0.31	5.35 ± 0.28
		$^{R}Q_1$	6.68 ± 0.27	3.92 ± 0.29
		$^{R}Q_4$	3.06 ± 0.16	5.49 ± 0.52
		$^{P}Q_1$	9.40 ± 0.27	5.03 ± 0.26
		$^{P}Q_3$	6.49 ± 0.19	5.22 ± 0.28
		$^{P}Q_4$	3.67 ± 0.22	4.55 ± 0.50
1997 Apr. 6.2	BS 2560 (15 Lyn)	$^{R}Q_0 + {}^{P}Q_1$	31.54 ± 0.76	7.05 ± 0.71
1997 Apr. 8.1	BS 2560	$^{R}Q_0$	11.48 ± 0.32	5.10 ± 0.27
		$^{R}Q_0$	15.08 ± 0.59	6.71 ± 0.49
		$^{R}Q_0$	11.03 ± 0.33	4.90 ± 0.27
		$^{R}Q_2$	9.08 ± 0.27	5.79 ± 0.32
		$^{R}Q_4$	5.83 ± 0.31	5.77 ± 0.58
		$^{R}Q_4$	5.80 ± 0.23	5.75 ± 0.43
		$^{P}Q_1$	11.71 ± 0.33	5.86 ± 0.31
		$^{P}Q_1$	11.24 ± 0.46	5.61 ± 0.43
		$^{P}Q_1$	11.62 ± 0.33	5.81 ± 0.31
1997 Apr. 9.0	BS 2560	$^{R}Q_0$	15.89 ± 0.54	6.50 ± 0.41
		$^{R}Q_0$	14.61 ± 0.49	5.96 ± 0.37
		$^{R}Q_1$	13.02 ± 0.36	6.12 ± 0.31
		$^{R}Q_1$	12.20 ± 0.35	5.74 ± 0.30
		$^{R}Q_2$	12.91 ± 0.43	7.93 ± 0.49
		$^{R}Q_2$	10.89 ± 0.37	6.69 ± 0.42
		$^{R}Q_4$	4.38 ± 0.25	4.58 ± 0.48
		$^{R}Q_4$	5.79 ± 0.20	6.07 ± 0.38
		$^{P}Q_1$	13.20 ± 0.44	6.04 ± 0.37
		$^{P}Q_1$	12.34 ± 0.41	5.65 ± 0.34
		$^{P}Q_2$	11.48 ± 0.34	5.50 ± 0.30
		$^{P}Q_2$	10.24 ± 0.40	4.92 ± 0.36
		$^{P}Q_3$	8.37 ± 0.29	5.15 ± 0.32
		$^{P}Q_3$	10.01 ± 0.39	6.17 ± 0.44
1997 Apr. 10.2	BS 2560	$^{R}Q_0 + {}^{P}Q_1$	26.82 ± 0.55	6.28 ± 0.63
1997 Apr. 30.0	BS 2560 and BS 8781 (α Peg)	$^{R}Q_0$	8.60 ± 0.34	5.73 ± 0.42
		$^{R}Q_0$	10.20 ± 0.29	6.78 ± 0.35
		$^{R}Q_1$	7.80 ± 0.31	5.87 ± 0.43
		$^{R}Q_1$	8.64 ± 0.25	6.49 ± 0.34
		$^{R}Q_2$	6.63 ± 0.28	6.33 ± 0.49
		$^{R}Q_2$	7.74 ± 0.22	7.38 ± 0.40
		$^{R}Q_4$	4.46 ± 0.23	6.68 ± 0.63
		$^{R}Q_4$	4.48 ± 0.19	6.70 ± 0.51
		$^{P}Q_1$	7.00 ± 0.27	5.22 ± 0.37
		$^{P}Q_1$	9.97 ± 0.28	7.46 ± 0.40
		$^{P}Q_2$	8.06 ± 0.23	6.23 ± 0.33
		$^{P}Q_3$	8.24 ± 0.23	7.93 ± 0.42
1997 May 1.2	BS 2560 and BS 8781	$^{R}Q_0$	7.22 ± 0.29	4.35 ± 0.32
		$^{R}Q_0$	9.54 ± 0.27	5.74 ± 0.30
		$^{R}Q_1$	7.91 ± 0.22	5.51 ± 0.29
		$^{R}Q_2$	5.77 ± 0.17	5.29 ± 0.29
		$^{R}Q_4$	3.23 ± 0.13	5.21 ± 0.38
		$^{P}Q_1$	5.22 ± 0.21	3.52 ± 0.27
		$^{P}Q_1$	6.81 ± 0.19	4.58 ± 0.24

TABLE III—*Continued*

UT date	Infrared flux standard stars[a]	Q-branch[b]	Line flux (10^{-17} W m^{-2})[d]	Q (C_2H_6) (10^{28} mol s^{-1})[f]
1997 Aug. 7.9	BS 1165 and BS 3903 (ν^1 Hya)	$^RQ_0 + {}^PQ_1$	0.61 ± 0.09	0.65 ± 0.17
1997 Aug. 8.8	BS 1165 and BS 3903	$^RQ_0 + {}^PQ_1$	0.77 ± 0.08	0.82 ± 0.15
1997 Sep. 25.7	BS 1165	$^RQ_0 + {}^PQ_1$	0.11 ± 0.02[e]	0.46 ± 0.15[g]

[a] BS numbers are given with the star name in parentheses. The same calibration stars were used for each grating setting on a particular date.
[b] Lines repeated in the table indicate separate measurements.
[c] When only the $^RQ_0$ and $^PQ_1$ Q-branches were detected, the sum of their fluxes are reported.
[d] Total transmittance corrected flux 2–12 arcsec off the nucleus in both the east and west directions unless otherwise noted.
[e] Total transmittance corrected flux in a 1 × 1-arcsec^2 box centered on the nucleus.
[f] Production rates derived by stepping 1 × 1-arcsec^2 extracts between 2 and 12 arcsec off the nucleus at 1-arcsec intervals in both the east and west directions for each measured line unless otherwise noted.
[g] Production rate derived from a 1 × 1-arcsec^2 box centered on the nucleus (see text).

of a photon with wavenumber ν (cm^{-1}), $f(x)$ is the fraction of molecules expected in the sampled region (x being the fraction of a photodissociation scale length subtended by the beam radius; see Appendix of Hoban *et al.* (1991)), and F_i is the flux (W m^{-2}) from the ith Q-branch incident atop the terrestrial atmosphere. A small correction factor (15%) is applied to account for flux that falls outside the five-columns extracted for a given Q-branch (the image of a spectral line is slightly broader than the 1-arcsec slit width). Transmittance-corrected fluxes are given in Table III for each measured ethane Q-branch.

We adopted a gas outflow velocity consistent with measurements at radio wavelengths for Hale–Bopp ($v_{gas} = 1.1 R_h^{-0.5}$ km s^{-1}; cf. Biver *et al.* (1999)), and took the standard photodissociation lifetime for quiet Sun conditions ($\tau_{C_2H_6} = 9.1 \times 10^4$ s; Huebner *et al.* (1992)). Dust Q-curves were generated using the simultaneously obtained continuum profile and assuming $\tau_{dust} \gg \tau_{C_2H_6}$ (Fig. 5B). "Symmetric" production rates were determined from each ethane Q-branch (Fig. 5C) by taking a weighted mean of corresponding spherical production rates east and west of the nucleus (Q_{dust} is scaled to $Q_{C_2H_6}$ at the first step (1 arcsec) off the nucleus in Fig. 5C).

The Q-curves for dust and C_2H_6 (as well as other volatile species) show that production rates derived from nucleus-centered extracts are lower than those derived at positions offset from the nucleus, due to seeing, drift, and other factors associated with real observing conditions (see Dello Russo *et al.* (1998,

TABLE IV
Rotational Temperatures, Production Rates, and Relative Abundances for Ethane in Comet Hale–Bopp

UT date	$Q(C_2H_6)$ (10^{28} molec s^{-1})	T_{rot}	$Q(H_2O)$[b] (10^{30} molec s^{-1})	C_2H_6/H_2O (10^{-3})	$Q(C_2H_2)$[c] (10^{28} molec s^{-1})	C_2H_6/C_2H_2
1996						
Jun 12.6	<0.6	20[a]				
Sep 20.3	0.29 ± 0.12	30[a]				
Dec 11.1	0.79 ± 0.20	50[a]				
1997						
Jan 21.8	2.15 ± 0.47	70[a]	4.00 ± 0.39	5.38 ± 1.29		
Feb 24.0	5.00 ± 0.42	78^{+30}_{-22}	8.89 ± 0.89	5.62 ± 0.73	3.4 ± 0.6	1.5 ± 0.3
Apr 6.2	7.05 ± 0.71	128[a]	10.69 ± 1.07	6.59 ± 0.93	3.4 ± 1.3	2.1 ± 0.8
Apr 8.1	5.63 ± 0.48	134^{+34}_{-28}	9.34 ± 0.93	6.03 ± 0.79		
Apr 9.0	5.99 ± 0.72	112^{+54}_{-40}	9.33 ± 0.54	6.42 ± 0.86		
Apr 10.2	6.28 ± 0.63	128[a]	9.99 ± 0.38	6.29 ± 0.67		
Apr 30.0	6.71 ± 0.75	133^{+53}_{-42}	6.76 ± 0.33	9.93 ± 1.21	2.4 ± 0.2	2.8 ± 0.4
May 1.2	5.03 ± 0.65	107^{+46}_{-37}	7.43 ± 0.41	6.77 ± 0.95	1.6 ± 0.7	3.1 ± 1.4
Aug 7.9	0.65 ± 0.17	50[a]	<1.5	$>4.3 \pm 1.1$		
Aug 8.8	0.82 ± 0.15	50[a]				
Sep 25.7	0.46 ± 0.15	30[a]				

[a] Adopted rotational temperatures. (On UT Apr. 6.2 and Apr. 10.2 adopted values were based on a weighted average of derived values for Apr. 8.1 and Apr. 9.0.)
[b] Values taken from Dello Russo *et al.* (2000).
[c] Values taken from Magee-Sauer *et al.* (2001, in preparation).

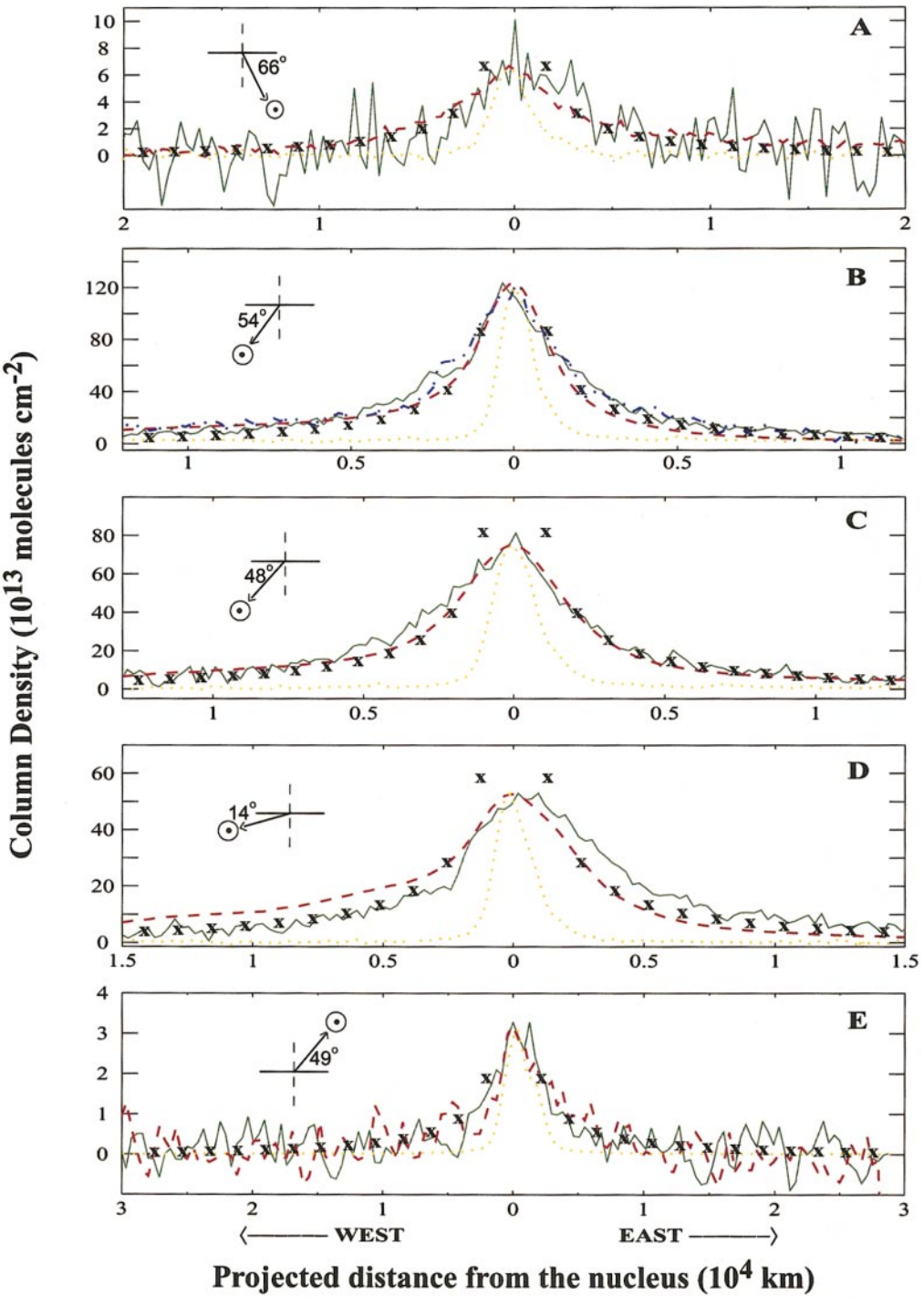

FIG. 4. Spatial profiles for C_2H_6 and dust in Comet Hale–Bopp on five dates: (A) UT 1997 Jan. 21.8, (B) UT 1997 Apr. 6.2, (C) UT 1997 Apr. 9.0, (D) UT 1997 May 1.2, and (E) UT 1997 Aug. 8.8. The C_2H_6 column densities (green solid curves), the continuum profiles (red dashed curves), and stellar profiles (PSFs, yellow dotted curves) are displayed. A scaled spatial profile for water is also shown (blue curve with alternating dots and dashes) in (B). A ρ^{-1} distribution (x′s) is also shown at intervals of 1 arcsec on all plots. The C_2H_6 profiles incorporate all Q-branches measured on a particular date. We note that spatial profiles for individual Q-branches on a particular date were similar. The slit was oriented east–west on all dates. The direction of the Sun with respect to the comet is indicated with a compass on the left side of each figure.

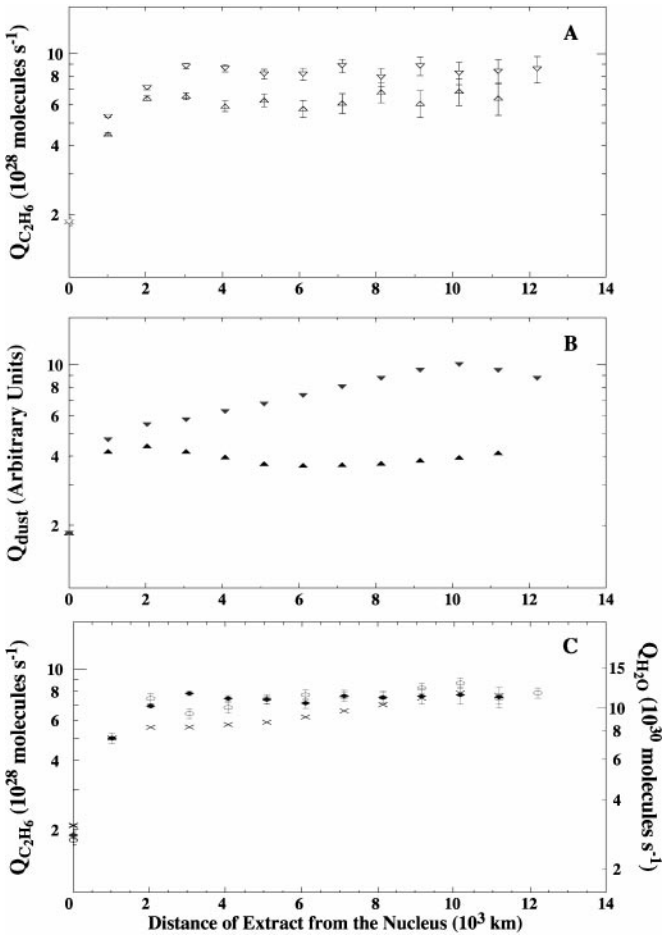

FIG. 5. Production rate growth curves (Q-curves) for C_2H_6 and dust in Comet Hale–Bopp on UT 1997 Apr. 6.2. (A) Ethane Q-curve: Ethane spherical production rates derived by stepping 1×1-arcsec^2 extracts east (open triangles pointing up) and west (open triangles pointing down) of the nucleus out to a distance of $\sim 1.2 \times 10^4$ km (12 arcsec). (B) Continuum Q-curve: Dust spherical production rates east (filled triangles pointing up) and west (filled triangles pointing down) of the nucleus (errors in spherical production rates for the dust are smaller than the size of the plotted points). (C) Symmetric Q-curves for C_2H_6 (diamonds), dust (crosses), and H_2O (open circles) derived from a weighted average of east and west extracts (for comparison, the dust and water production rates are scaled to the ethane production rate at the first step (1 arcsec) off the nucleus).

2000) for detailed discussion). Typically, symmetric production rates reached a constant (terminal) value near 2 arcsec from the nucleus, and nucleus-centered values were about a factor of 3–4 lower than terminal values (Fig. 4C). For this reason, for the 11 dates when $R_h \leq 2.25$ AU, the "global" production rate determined from each individual Q-branch of C_2H_6 was taken from a weighted average of symmetric production rates over the range 2–12 arcsec from the nucleus. Although asymmetries will likely have a small residual effect on our global production rates, this method has been shown to be a valid approach to first order (cf. Xie and Mumma 1996). On UT 1996 Sep. 20.3 and 1997 Sep. 25.7, the signal-to-noise ratio between 2 and 12 arcsec from the nucleus was too small to measure the flux accurately. On these dates production rates were determined from the observed flux in a 1×1-arcsec^2 box centered on the nucleus scaled upward by a factor of 3 (Table III). Global production rates for a particular date (Table IV) are represented by the weighted average of values obtained from individual Q-branch measurements on that date, as listed in Table III. Although detected on multiple dates (Fig. 3A; Table I), the $^RQ_3$ Q-branch was not used in this analysis since it is blended with lines of CH_3OH and OH whose intensities are not known.

Errors were evaluated on each date for all detected Q-branches. The (1σ) errors in Q-branch flux reported in Table III were derived from the deviation of the C_2H_6 spatial profile (Fig. 3) from a fitted curve (Gaussian + polynomial). For each Q-branch in Table III within $R_h = 1.49$ AU, the uncertainty in the global production rate was dominated by the standard deviation of the mean production rate over the range 2–12 arcsec from the nucleus (e.g. Fig. 5C). This includes factors such as deviations in the synthetic atmospheric model fit, instrumental effects, spatial variations in rotational temperature and outflow velocity, and other factors that cause deviations from our idealized gas outflow model. For $R_h \geq 1.49$ AU, the uncertainty in the global production rate was dominated by photon noise (stochastic error). Possible errors in the fluorescence model (e.g., uncertainty in excited-state → ground-state branching ratios and the ν_7 band g-factor) were not included. On dates where only the $^RQ_0$ and $^PQ_1$ Q-branches were detected and a rotational temperature was not determined, a minimum uncertainty of 10% in the production rate was assumed.

Our ethane production rates are shown vs heliocentric distance in Fig. 6. A least-squares fit to values on 11 dates yielded $Q_{C_2H_6} = (5.52 \pm 0.20) \times 10^{28}$ $[R_h^{(-2.43\pm0.13)}]$ molecules s^{-1}, which is close to (but slightly steeper than) the insolation-limited dependence of R_h^{-2}. Separate pre- and post-perihelion dependences for C_2H_6 give $R_h^{(-3.01\pm0.33)}$ and $R_h^{(-2.34\pm0.18)}$ respectively. Somewhat flatter heliocentric dependences were derived for production of native CO ($R_h^{(-1.73\pm0.26)}$ between 4.1 and 0.9 AU; DiSanti *et al.* (1999)), H_2O ($R_h^{(-1.88\pm0.18)}$ between 1.5 and 0.9 AU; Dello Russo *et al.* (2000)), and dust at millimeter wavelengths ($R_h^{(-1.7\pm0.2)}$ between 2.5 and 0.9 AU, Jewitt and Matthews (1999)).

The different heliocentric dependences derived for C_2H_6 and H_2O should be interpreted with caution. Although this difference superficially suggests that ethane release is not controlled by water sublimation, production rates for H_2O were only measured directly by us for $R_h \leq 1.49$ AU, and a steeper dependence is likely between 1.5 and 3 AU where release of H_2O is not insolation-limited (cf. Weaver *et al.* 1999b). In fact, the heliocentric dependence for C_2H_6 when $R_h \leq 1.49$ AU ($R_h^{(-1.66\pm0.34)}$) is the same within error as that derived for H_2O. Therefore, our data are not inconsistent with ethane production being controlled by water sublimation.

Despite apparent differences in the derived heliocentric dependences pre- and post-perihelion for C_2H_6, the evidence for pre- and post-perihelion asymmetries is not compelling. The

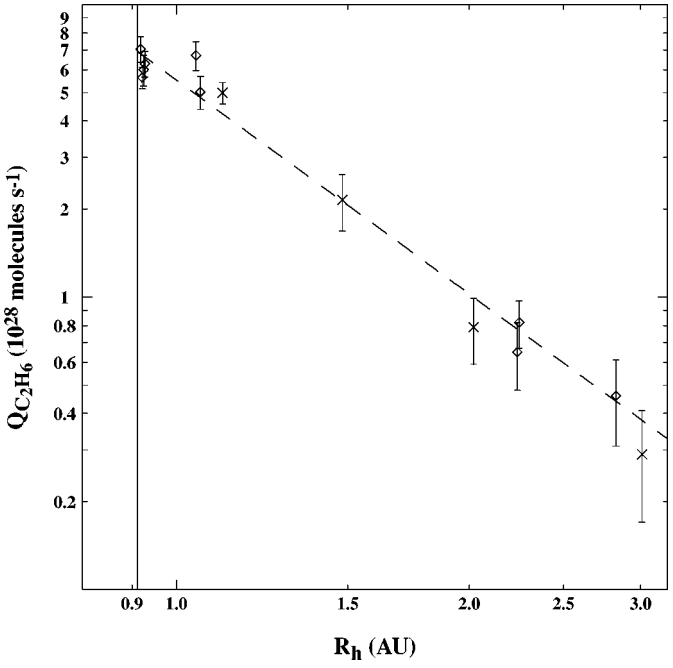

FIG. 6. Evolution of the C_2H_6 production rate in Comet Hale–Bopp with heliocentric distance R_h. The solid vertical line represents the heliocentric distance at perihelion. The dashed line is the heliocentric dependence $Q = (5.52 \pm 0.20) \times 10^{28}$ $[R_h^{(-2.43\pm0.13)}]$ molecules s^{-1}, derived from a least-squares fit to our measured values pre-perihelion (crosses) and post-perihelion (diamonds). Separate pre- and post-perihelion dependences for ethane give $R_h^{(-3.01\pm0.33)}$ and $R_h^{(-2.34\pm0.18)}$ respectively. Based on our fit, we estimate the absolute 1σ uncertainty in $Q_{C_2H_6}$ to be $\pm0.73 \times 10^{28}$, $\pm0.16 \times 10^{28}$, and $\pm0.75 \times 10^{27}$ at 1.0, 2.0, and 3.0 AU, respectively.

post-perihelion fit is strongly influenced by the four measurements near perihelion while there are no measurements within 1.11 AU pre-perihelion (Fig. 6). Furthermore, our derived production rates for $R_h \geq 1.11$ AU suggest a flatter heliocentric dependence near perihelion (Fig. 6). Neglecting the four measurements near perihelion, our post-perihelion dependence ($R_h^{(-2.69\pm0.21)}$) is not significantly different from the derived pre-perihelion dependence ($R_h^{(-3.01\pm0.33)}$). Unfortunately, significant gaps in our heliocentric coverage within 3 AU prevent us from definitively concluding that ethane release is controlled by water sublimation. While we find no compelling evidence for pre- and post-perihelion asymmetries in C_2H_6 production, these gaps also limit our ability to test possible asymmetries in production. These gaps could also mask a more complex behavior for C_2H_6 than is implied by a single heliocentric dependence fit within 3 AU.

6. THE IMPLICATIONS OF ABUNDANT ETHANE IN COMETS

How common are ethane-rich comets? Prior to the advent of high-resolution ground-based infrared spectroscopy, C_2H_6 had not been detected in comets. This is not surprising since C_2H_6 Q-branch emissions could not be resolved and differentiated from other organic species (most notably methanol) in the 3.35-μm region with the moderate-resolution spectrometers then available (e.g., compare the high- and moderate-resolution spectra of Comet Lee shown in Figs. 1 and 2 of Mumma *et al.* (2001a)). Five Oort cloud comets (Hyakutake, Hale–Bopp, Lee, C/1999 S4 LINEAR, and C/1999 T1 McNaught–Hartley) have been observed since high-resolution ground-based infrared spectrometers became available, and C_2H_6 has been detected in four of them with very similar abundances (relative to water, Table V). The only exception was Comet LINEAR, which was severely depleted in C_2H_6 as well as many other volatile species (Mumma *et al.* 2001b). Since C_2H_6 has only been sampled in only a few Oort cloud comets, the extent and frequency of such variations are not yet clear. The data obtained so far suggest the presence of abundant C_2H_6 (relative to CH_4 and C_2H_2) in Oort cloud comets may be the rule rather than the exception.

The C_2H_2 observed in comets was likely formed by gas-phase ion-molecule reactions in the natal interstellar cloud core, but C_2H_6 cannot be formed in this way because one critical reaction is energetically forbidden. It was suggested that C_2H_6 could be produced on icy grains in the natal cloud, either by photolysis of CH_4 ice or by hydrogen atom addition reactions to C_2H_2 condensed from the gas phase (Mumma *et al.* 1996). Comparison of the relative abundances of these chemically linked species may be important in constraining cometary formation scenarios. Similar relative amounts of these species in Comets Hyakutake, Hale–Bopp, and Lee (Table V) are consistent with

TABLE V
Relative Ethane Abundances in Five Oort Cloud Comets

Comet	C_2H_6/H_2O	C_2H_6/C_2H_2	C_2H_6/CH_4
C/1996 B2	$(6.4 \pm 1.5) \times 10^{-3}$ [a]	$\sim$0.5–4[c]	$\sim$0.5[b]
Hyakutake	(4–12)$\times 10^{-3}$[b]	4 ± 2[d]	
C/1995 O1 Hale–Bopp	$(6.23 \pm 0.42) \times 10^{-3}$[e]	2.4 ± 0.7[f]	0.55[g]
C/1999 H1 Lee	$(7.1 \pm 0.7) \times 10^{-3}$[h]	2.6 ± 0.3[h]	0.88 ± 0.12[h]
C/1999 S4 LINEAR	$(1.3 \pm 0.2) \times 10^{-3}$[i]	>0.9[i]	0.87 ± 0.18[i]
C/1999 T1 McNaught–Hartley	6.5×10^{-3}[j]		>0.4[j]

[a] Dello Russo *et al.* (1999), for UT 1996 Mar 24.5.
[b] Mumma *et al.* (1996), for UT 1996 Mar 24.5.
[c] Based on relative abundances reported in Mumma *et al.* (1996) (UT 1996 Mar 24.5) and Brooke *et al.* (1996) (UT 1996 Apr 8.2).
[d] Dello Russo *et al.* (1999), and Magee-Sauer *et al.* (2001, in preparation) for UT 1996 Mar 24.5.
[e] This work. Based on a weighted average of all dates in Table IV except UT 1997 Apr 30.0. Including all dates $C_2H_6/H_2O = (6.7 \pm 1.4) \times 10^{-3}$.
[f] This work, and Magee-Sauer *et al.* (2001, in preparation) based on a weighted average of four dates (see Table IV).
[g] Weaver *et al.* (1999a), for UT 1997 Mar 1.9.
[h] Mumma *et al.* (2001a), for UT 1999 Aug 21.6.
[i] Mumma *et al.* (2001b), for UT 2000 July 13.6.
[j] Preliminary values from Mumma *et al.* (2001c), IAU Circular 7578, for UT 2001 Jan 14.7.

a common chemical origin. This could reflect creation by kinetically controlled production processes in the natal cloud core. Alternatively, they could have formed in a common region of the solar nebula (whether from thermochemically equilibrated species or as a result of hydrogenation of icy grains is not yet clear). The detection of C_2H_6 with depleted abundance in probable Kuiper-belt Comet Giacobini-Zinner (Weaver *et al.* 1999c, Mumma *et al.* 2000) may reflect different processing of precometary ices in the transneptunian nebular region. These data imply a link between the processing histories of precometary ices and the relative abundances of these species in comets. However, the depletion of native CO in Comet Lee by about a factor of 5 to 10 with respect to Hyakutake and Hale–Bopp (Mumma *et al.* 2001a) shows that many questions remain. A better understanding of processing in the early solar nebula will be obtained as the chemistry of more comets is studied.

Laboratory studies have yielded interesting and relevant results that can be compared to measured cometary abundances to help constrain formation scenarios. If the C_2H_6 in Comet Hale–Bopp was produced entirely via H atom addition reactions to C_2H_2, the conversion proceeded with high efficiency ($\sim$60–75%). Ethane can be produced with these high efficiencies from hydrogen atom addition reactions on C_2H_2 and ethylene (C_2H_4) ices (Hiraoka *et al.* 2000), but the efficiency of this process depends strongly on temperature. Ethane yields increase dramatically with a decrease in temperature from 50 to 10 K, presumably due to increased sticking probabilities of H atoms at lower temperatures (Hiraoka *et al.* 2000). Interestingly, Hiraoka *et al.* showed that hydrogen atom addition reactions to C_2H_2 do not form detectable amounts of the intermediate C_2H_4 even though C_2H_4 is not completely converted to C_2H_6 when it is the starting ice. If H atom addition reactions play an important role in shaping the composition of precometary ices, C_2H_4 may be depleted in comets relative to C_2H_2 and C_2H_6. Thus, determining the C_2H_4 abundance in comets (or even obtaining a meaningful upper limit) may provide a key test of the importance of H atom addition reactions in cometary formation scenarios.

Ethylene was searched for but not detected in Comets Hyakutake and Hale–Bopp. Several factors make detecting C_2H_4 (or even determining an upper limit) problematic. C_2H_4 has two fundamental bands at $\sim$2988.6 (ν_{11}) and 3104.9 cm^{-1} (ν_9), both of which are significantly weaker than the ν_7 band of C_2H_6 and the ν_3 band of C_2H_2 (the ν_9 and ν_{11} bands of C_2H_4 each have band g-factors at 1 AU of $\sim 1 \times 10^{-4}$ s^{-1}, based on band intensities given by Dang-Nhu *et al.* (1983)). The perpendicular ν_9 band has several Q- branches, but the atmosphere has generally low transmittance near 3100 cm^{-1}, making detection difficult. The ν_{11} parallel band has a strong Q-branch near 2988.6 cm^{-1}, but three factors make its detection problematic: (1) The Q-branch is relatively broad ($\sim$1 cm^{-1} wide; Van Lerberghe *et al.* (1972)), spreading any on-chip intensity over many pixels. (2) The Q-branch position is coincident with a region of strong telluric methane and water lines that together cause generally poor transmittance. (3) Any emission intensity from C_2H_4 must be separated from the ubiquitous (and largely unmodeled) CH_3OH emissions in this spectral region. Another complicating factor is that line intensities for C_2H_4 are not known due to the absence of low-temperature, line-by-line fluorescence models for these bands (analysis of C_2H_4 in this spectral region is complicated by the presence of numerous combination bands, Sartakov *et al.* (1997)). For these reasons an upper limit for C_2H_4 in Hale–Bopp was not determined, and the C_2H_4 abundance in comets remains unknown.

In an alternate view, Notesco *et al.* (1997) showed that relative abundances of C_2H_6 and CH_4 comparable to those found in Hyakutake (and Hale–Bopp) can be simulated in the laboratory by trapping these gases in water ice at $\sim$65 K. In addition to C_2H_6, Notesco *et al.* also predict the presence of propane (C_3H_8) with an abundance comparable to CH_4 and C_2H_6 (C_2H_6/C_3H_8 $\sim$1.5–2), if precometary ice formed by condensation of nebular gas in some regions at $\sim$65 K. However, other evidence supports a formation temperature of $\sim$30 K in Hale–Bopp (Crovisier *et al.* 1997, Krasnopolsky *et al.* 1997, Meier *et al.* 1998a,b; Stern *et al.* 2000). C_3H_8 was not detected in Comets Hyakutake and Hale–Bopp. However, as with C_2H_4, isolation of possible C_3H_8 emission from CH_3OH is difficult even at high resolution, and adequate line-by-line fluorescence models do not exist. Both C_3H_8 and CH_3OH have several infrared-active fundamental bands in the C–H stretch spectral region that give rise to a dense grouping of lines. Since C_3H_8 may be at least a factor of 10 less abundant than CH_3OH in comets, differentiation of any propane features from weak methanol lines requires the development of low-temperature line-by-line fluorescence models for all strong bands of C_3H_8 and CH_3OH in the region 3.3–3.6 μm. Thus, an upper limit for C_3H_8 was not obtained in Hale–Bopp and the C_2H_6/C_3H_8 ratio in comets remains an open question.

The presence of abundant cometary C_2H_6 has implications for the origin of the 3.2–3.6 μm X–CH feature seen in many comets when observed at low ($\lambda/\Delta\lambda \sim 100$) and medium ($\lambda/\Delta\lambda \sim$ 1000) spectral resolving power (cf. Bockelée-Morvan *et al.* 1995). That C_2H_6 could contribute to this feature in comets became evident following its discovery in Hyakutake (cf. Mumma *et al.* 1996, Crovisier 1999). The combined g-factors at 1 AU from the Sun for fundamental bands of CH_3OH and C_2H_6 in this region are $\sim 7 \times 10^{-4}$ and 9×10^{-4} s^{-1} respectively (including the ν_2, ν_9, and ν_3 bands of methanol, Rogers (1980); including the ν_5 and ν_7 bands of ethane, Dang-Nhu *et al.* (1984)). Assuming a mixing ratio of $C_2H_6/CH_3OH \sim 0.1$–1.0 in comets, the ethane contribution to the X–CH feature is significant ($\sim$10–130% of the total contribution from methanol, slightly less if methanol overtone and combination bands contribute significantly in this region). This is consistent with earlier conclusions that CH_3OH (ν_2 and ν_9) could contribute only up to $\sim$50–60% of the 3.4-μm "cometary organic" emission feature observed in several comets (Reuter 1992, Bockelée-Morvan *et al.* 1995).

7. SUMMARY

The detection of C_2H_6 in comets provides another valuable clue to the origin and processing histories of cometary ices. Since production of C_2H_6 by gas-phase ion–molecule reactions is energetically forbidden, the discovery of abundant C_2H_6 in Comet Hyakutake implied its ices did not originate in this way (Mumma *et al.* 1996). However, the abundances of related hydrocarbons (e.g., CH_4, C_2H_2, CO, and CH_3OH) argued against formation in a thermochemically equilibrated region of the solar nebula. Mumma *et al.* (1996) suggested that C_2H_6 formed on icy grain mantles in the natal cloud by photolysis of CH_4 or by H atom addition reactions to C_2H_2. The apparition of Comet Hale–Bopp afforded an opportunity to measure the relative abundances of these potentially interrelated species in a bright comet with high spectral and spatial resolution over a large range in heliocentric distance.

Multiple Q-branches of C_2H_6 were detected in Hale–Bopp on 13 dates between UT 1996 September 20.3 and 1997 September 25.7 (Tables I and II; Figs. 1, 2, 3). A simple fluorescence model for C_2H_6 was developed, enabling production rates to be measured (Tables III and IV). The heliocentric dependence derived for the C_2H_6 production rate in Hale–Bopp was $Q = (5.52 \pm 0.20) \times 10^{28}$ $[R_h^{(-2.43\pm0.13)}]$ molecules s^{-1} (Fig. 6). Although this heliocentric dependence for C_2H_6 is steeper than that measured for H_2O ($R_h^{(-1.88\pm0.18)}$), it is not inconsistent with ethane production being controlled by water sublimation since H_2O production was only measured for $R_h \leq 1.49$ AU, and a steeper dependence for H_2O is likely between 1.5 and 3 AU. The spatial distribution of C_2H_6 molecules in the coma was consistent with all C_2H_6 being released directly from the nucleus for all distances within 3.01 AU of the Sun (Fig. 4), although it is possible that a small fraction was released as a distributed source. When our derived ethane, water, and acetylene production rates are compared, we obtain $C_2H_6/H_2O = (6.23 \pm 0.42) \times 10^{-3}$, and $C_2H_6/C_2H_2 = 2.4 \pm 0.7$ (Tables IV and V). If C_2H_6 in Hale–Bopp was produced entirely via H atom addition reactions to C_2H_2, this implies the conversion of $C_2H_2 \rightarrow C_2H_6$ proceeded with ~60–75% efficiency.

Comparison of three Oort cloud comets (Hyakutake, Hale–Bopp, and Lee) shows remarkably similar relative abundances for C_2H_6, C_2H_2, CH_4, and H_2O (Table V), implying that these three comets experienced similar processing histories. Abundances and upper limits for C_2H_4 and C_3H_8 (species that may also be chemically linked to C_2H_6, C_2H_2, and CH_4) were not obtained in Hyakutake or Hale–Bopp due to the lack of low-temperature line-by-line fluorescence models and difficulties associated with detecting emission from these species. However, there was no clear evidence of excess emission at the frequencies expected for lines of C_2H_4 or C_3H_8.

The detection of C_2H_6 in five Oort cloud comets observed with ground-based high-resolution spectroscopy demonstrates that abundant C_2H_6 (relative to CH_4 and C_2H_2) in comets may be the rule rather than the exception. This has implications for the origin of the 3.2–3.6 μm X–CH feature seen in many comets with low and medium resolution (cf. Reuter 1992, DiSanti *et al.* 1995, Bockelée-Morvan *et al.* 1995), suggesting that C_2H_6 should at least partially account for the unexplained excess emission in this region that cannot be attributed to CH_3OH. C_2H_6 production rates obtained from a systematic study of comets at infrared wavelengths will continue to be important in constraining the origin and processing histories of cometary ices.

APPENDIX

Determination of Ethane ν_7 g-Factors

Although C_2H_6 is a simple hydrocarbon with high symmetry (D_{3d}), it possesses a dense and complex rotational fine structure in its infrared bands. The goal of this study was to develop a simple fluorescence model for C_2H_6 as a function of temperature. As an example of how g-factors were determined, we will show the calculation for the ${}^pQ_1$ Q-branch at 100 K.

A. Determination of the Ground-State Populations

The energy of a prolate symmetric top molecule including vibrational and rotational interactions and centrifugal distortion is given in Herzberg (1945):

$$E(J,K) = B_0 J(J+1) + (A_0 - B_0)K^2 - D_0^J J^2(J+1)^2 - D_0^{JK} K^2 J(J+1) - D_0^K K^4.$$

In this equation Coriolis coupling and all higher order vibration–rotation interactions as well as possible l-type doubling effects are neglected. Constants (in cm^{-1}) are as follows (Pine and Lafferty 1982):

$$B_0 = 0.663, \quad A_0 = 2.671, \quad D_0^J = 1.03 \times 10^{-6}, \quad D_0^{JK} = 2.66 \times 10^{-6}, \quad D_0^K = 1.09 \times 10^{-5}$$

The rotational partition function can be approximated if centrifugal distortion terms are neglected:

$$Z_r \sim \sum_{J=0}^{\infty} \sum_{K=-J}^{+J} \varepsilon_{JK}(2J+1) \exp\left[\frac{-hc}{kT}\{B_0 J(J+1) + (A_0 - B_0)K^2\}\right].$$

The initial ground-state populations are defined by the statistical weights of the rotational levels that are split into doublets. The torsionally split rotational levels and their statistical weights (ε_{JK}) are given below (Wilson 1938, Dang-Nhu *et al.* 1984):

For K not a multiple of 3: $\varepsilon_{JK} = 4$ for $\psi_{JK} = A$ or B;

$\varepsilon_{JK} = 16$ for $\psi_{JK} = E_1$ or E_2

For K a multiple of 3, but $\neq 0$: $\varepsilon_{JK} = 16$ for $\psi_{JK} = A$ or B;

$\varepsilon_{JK} = 8$ for $\psi_{JK} = E_1$ or E_2

For $K = 0$ and $J =$ even: $\varepsilon_{JK} = 6$ for $\psi_{JK} = A$;

$\varepsilon_{JK} = 2$ for $\psi_{JK} = E_1$

For $K = 0$ and $J =$ odd: $\varepsilon_{JK} = 10$ for $\psi_{JK} = A$;

$\varepsilon_{JK} = 6$ for $\psi_{JK} = E_1$

In the limit $B_0 hc/k \ll T$ (in this case $B_0 hc/k \sim 1$ K), the rotational partition

function can be expressed as

$$Z_r \sim 11\sqrt{\pi}\left(\frac{k}{hc}\right)^{3/2}\left(\frac{T}{B_0}\right)\left(\frac{T}{A_0}\right)^{1/2}.$$

Since C_2H_6 has a low-frequency torsional mode (ν_4) at $\nu \sim 290$ cm^{-1}, the vibrational partition function may contribute significantly to the total partition function for temperatures experienced in Hale–Bopp near perihelion. Assuming the populations in all other excited vibrational states except ν_4 are zero, the vibrational partition function can be calculated:

$$Z_v = \left[1 - \exp\left(-\frac{hc\nu_4}{kT}\right)\right]^{-1}.$$

The total partition function is then expressed as $Z = Z_r Z_v$.

For this analysis we treat the unresolved torsionally split rotational levels as a single state. The initial population in a specific ground-state rotational level can then be calculated:

$$\begin{aligned}
N_{JK} &= 20(2J+1)\exp[-hc/kT\{B_0 J(J+1) \\
&\quad + (A_0 - B_0)K^2\}] \quad \text{for } K \text{ not a multiple of 3.} \\
N_{JK} &= 24(2J+1)\exp[-hc/kT\{B_0 J(J+1) \\
&\quad + (A_0 - B_0)K^2\}] \quad \text{for } K \text{ a multiple of 3.} \\
N_{JK} &= 8(2J+1)\exp[-hc/kT\{B_0 J(J+1) \\
&\quad + (A_0 - B_0)K^2\}] \quad \text{for } K = 0,\ J = \text{even.} \\
N_{JK} &= 16(2J+1)\exp[-hc/kT\{B_0 J(J+1) \\
&\quad + (A_0 - B_0)K^2\}] \quad \text{for } K = 0,\ J = \text{odd.}
\end{aligned}$$

Now the initial fractional population (f_{JK}) in a particular ground-state rotational level at a certain temperature can be determined,

$$f_{JK} = N_{JK}/Z.$$

For the case of $^PQ_1$, the $K = 1$ fractional ground-state populations are needed and were calculated up to $J = 52$. They are listed in Table A.I for 100 K from $J = 1$ to 20. At 100 K, the fractional population in the ground state $K = 1$ level (for $J \geq K$, summed over all levels in $K = 1$) is 0.191.

TABLE A.I
Fractional Ground-State Populations for $K = 1$ at 100 K

J	E_{JK} (cm^{-1})	f_{JK}
1	3.33	0.00540
2	5.99	0.00867
3	9.96	0.01146
4	15.27	0.01365
5	21.90	0.01516
6	29.86	0.01598
7	39.14	0.01613
8	49.75	0.01569
9	61.68	0.01477
10	74.94	0.01348
11	89.52	0.01197
12	105.43	0.01035
13	122.66	0.00872
14	141.21	0.00717
15	161.09	0.00575
16	182.29	0.00451
17	204.82	0.00346
18	228.67	0.00259
19	253.84	0.00190
20	280.33	0.00136

B. Branching Ratios for the Pump from ν to ν'

The fractional branching ratios for the pump from a given lower state ($S_{J''K''}$) into the upper vibrational state ($S_{J'K'}$) for the ν_7 band are given by the Honl-London formulas for a perpendicular band (Herzberg 1945, Dang-Nhu *et al.* 1984):

$$BR = \frac{(J+2\pm K)(J+1\pm K)}{(J+1)(2J+1)}\left(\frac{F}{4}\right) \quad \text{for } \Delta J = +1 \text{ and } \Delta K = \pm 1,$$

$$BR = \frac{(J+1\pm K)(J\mp K)}{J(J+1)}\left(\frac{F}{4}\right) \quad \text{for } \Delta J = 0 \text{ and } \Delta K = \pm 1,$$

$$BR = \frac{(J-1\mp K)(J\mp K)}{J(2J+1)}\left(\frac{F}{4}\right) \quad \text{for } \Delta J = -1 \text{ and } \Delta K = \pm 1,$$

where,

$$F = \left[1 + \alpha K \Delta K + \beta \Delta J\left(J + \frac{1}{2} + \frac{\Delta J}{2}\right) + \cdots\right]^2,$$

$\alpha = 0.0144$, and $\beta = 0.0048$. For $K = 0$ and $\Delta K = +1$ the values given in the above formulas must be multiplied by 2. For the $^PQ_1$ transition we need to determine the branching ratios from $K'' = 1$ to $K' = 0$ (for all other Q-branches two sets of branching ratios must be considered, $K'' = K' \pm 1 \rightarrow K'$). Branching ratios for $^PQ_1$ ($K'' = 1, K' = 0$) and the fraction of the total molecules pumped to a specific upper state ($f_{J'K'}$) up to $J' = 20$ are shown in Table A.II.

C. Determination of g-Factors

Once $f_{J'K'}$ for each upper state is determined for a particular temperature, Q-branch emission g-factors can be determined from the band g-factor and branching ratios taken from $S_{J'K'}$ to $S_{J''K''}$. From the band intensity (I), the Einstein A coefficient (s^{-1}) can be calculated for the band. For C_2H_6 ν_7, we use $I_{\nu 7} = 1154$ cm^{-2} atm^{-1} at 115 K, derived from Dang-Nhu *et al.* (1984), who also report a value at 295 K (351.0 cm^{-2} atm^{-1}) using resolved, unperturbed transitions in the Doppler-limited spectrum (Pine and Lafferty 1982). This value was used in preference to $I_{\nu 7} = 548$ cm^{-2} atm^{-1} at 273 K derived from conversion of the measured integrated band area to band intensity in laboratory spectra with very low resolution (insufficient to resolve the ν_5 and ν_7 bands, Nyquist *et al.* (1957)). The Einstein A coefficient for ν_7 can be derived using the formalism given in Crovisier and Encrenaz (1983) and Crovisier (1984):

$$A_{\nu 7} = \frac{3.080 \times 10^{-8}\,(T/300)\nu^2 I_{\nu 7} Z_v}{\omega}.$$

This gives $A_{\nu 7} = 64.8$ s^{-1}, where ν is the wavenumber at band center (2985.39 cm^{-1}), T is the temperature (in Kelvin) at which the band intensity ($I_{\nu 7}$) was measured, Z_v is the vibrational partition function at temperature T, and ω is the degeneracy of the band. The Einstein A coefficient for ν_7 should be independent of temperature to first order, and we note that if $I = 351$ cm^{-2} atm^{-1} at 295 K is used, $A_{\nu 7} = 62.6$ s^{-1}. The g-factor for a fundamental vibrational band excited by a blackbody of solid angle Ω at temperature T_b can then

be determined (Crovisier and Encrenaz 1983):

$$g_{\nu 7} = \frac{\omega\Omega}{4\pi} A_{\nu 7} \left[\exp\left(\frac{hc\nu}{kT_b}\right) - 1\right]^{-1}.$$

For excitation by the Sun at 1 AU ($T_b = 5770$ K and $\Omega/4\pi = 5.42 \times 10^{-6}$), we obtain $g_{\nu 7} = 6.35 \times 10^{-4}$ s^{-1}. (If the band intensity from Nyquist *et al.* (1957) is used, $g_{\nu 7} = 8.56 \times 10^{-4}$ s^{-1}. Using this value would decrease our derived production rates by 35%.)

The branching ratios for emission from the excited state were determined in an analogous way to branching ratios for absorption (see section B above) (e.g., the parameters α and β are assumed to be the same for absorption and emission). From this we can obtain the fraction of molecules in the upper state that cascade into the lower state ($f_{J''K''}$), and emission g-factors for all unresolved J-lines within a given Q-branch. The sum of the g-factors for all J-lines within a given Q-branch gives the total g-factor for that Q-branch. An example is shown in Table A. III for $J'' = 1 \rightarrow 20$ lines of $^{P}Q_1$ at 100 K.

TABLE A.II
Fractional Branching Ratios for ($K'' = 1 \rightarrow K' = 0$) and $f_{J'K'}$ at 100 K

J''	J'	Fractional branching ratios	$f_{J'K'}$	J''	J'	Fractional branching ratios	$f_{J'K'}$
1	0	0.1587	0.00086	10	11	0.1269	0.00573
1	1	0.2404	0.00252	11		0.2401	
2		0.1415		12		0.1107	
1	2	0.0817	0.00405	11	12	0.1286	0.00497
2		0.2404		12		0.2400	
3		0.1334		13		0.1092	
2	3	0.0990	0.00536	12	13	0.1303	0.00421
3		0.2404		13		0.2400	
4		0.1284		14		0.1077	
3	4	0.1071	0.00640	13	14	0.1318	0.00348
4		0.2404		14		0.2399	
5		0.1248		15		0.1063	
4	5	0.1121	0.00712	14	15	0.1333	0.00281
5		0.2404		15		0.2398	
6		0.1220		16		0.1050	
5	6	0.1157	0.00752	15	16	0.1348	0.00222
6		0.2403		16		0.2397	
7		0.1196		17		0.1037	
6	7	0.1186	0.00761	16	17	0.1363	0.00171
7		0.2403		17		0.2396	
8		0.1175		18		0.1024	
7	8	0.1210	0.00743	17	18	0.1377	0.00129
8		0.2403		18		0.2395	
9		0.1156		19		0.1011	
8	9	0.1232	0.00701	18	19	0.1391	0.00095
9		0.2402		19		0.2394	
10		0.1138		20		0.0999	
9	10	0.1251	0.00643	19	20	0.1405	0.00069
10		0.2402		20		0.2393	
11		0.1122		21		0.0986	

TABLE A.III
$f_{J''K''}$ and g Factors for Ethane ν_7 $^{P}Q_1(J)$ Emissions at 100 K

J'	K'	J''	K''	$f_{J''K''}$	$g[^{P}Q_1(J)]$ (10^{-6} s^{-1})
1	0	1	1	0.00125	0.794
2	0	2	1	0.00201	1.27
3	0	3	1	0.00266	1.68
4	0	4	1	0.00317	2.01
5	0	5	1	0.00353	2.24
6	0	6	1	0.00372	2.36
7	0	7	1	0.00377	2.39
8	0	8	1	0.00368	2.33
9	0	9	1	0.00347	2.20
10	0	10	1	0.00318	2.02
11	0	11	1	0.00283	1.80
12	0	12	1	0.00246	1.56
13	0	13	1	0.00208	1.32
14	0	14	1	0.00172	1.09
15	0	15	1	0.00139	0.881
16	0	16	1	0.00109	0.694
17	0	17	1	0.000844	0.535
18	0	18	1	0.000636	0.403
19	0	19	1	0.000470	0.298
20	0	20	1	0.000339	0.215
Total contribution to $^{P}Q_1$				0.0450	28.5

ACKNOWLEDGMENTS

This work was supported by the NASA Planetary Atmospheres Program under NAG5-7753 to N. Dello Russo, by the NASA Planetary Astronomy Program under RTOP 344-32-30-07 to M. J. Mumma and Grant NAG5-7905 to M. A. DiSanti, and by the National Science Foundation under Grant AST-9619461 to K. Magee-Sauer. We thank T. Rettig for his participation in the observations. We also thank D. Schleicher and an anonymous referee for helpful comments. We are grateful for the outstanding support from the staff at the NASA Infrared Telescope Facility. The University of Hawaii operates the IRTF under contract to NASA.

REFERENCES

Biver, N., and 22 colleagues 1999. Long term evolution of the outgassing of Comet Hale-Bopp from radio observations. *Earth Moon Planets* **78**, 5–11 (1997).

Bockelée-Morvan, D., T. Y. Brooke, and J. Crovisier 1995. On the origin of the 3.2- to 3.6-μm emission features in comets. *Icarus* **116**, 18–39.

Bockelée-Morvan, D., P. Colom, J. Crovisier, D. Despois, and G. Paubert 1991. Microwave detection of hydrogen sulphide and methanol in Comet Austin (1989c1). *Nature* **350**, 318–320.

Brooke, T. Y., A. T. Tokunaga, H. A. Weaver, J. Crovisier, D. Bockelée-Morvan, and D. Crisp 1996. Detection of acetylene in the infrared spectrum of Comet Hyakutake. *Nature* **383**, 606–608.

Combes, M., and 18 colleagues 1986. Infrared sounding of Comet Halley from Vega 1. *Nature* **321**, 266–268.

Combes, M., and 16 colleagues 1988. The 2.5–12 μm spectrum of Comet Halley from the IKS-VEGA experiment. *Icarus* **76**, 404–436.

Crovisier, J. 1984. The water molecule in comets: Fluorescence mechanisms and thermodynamics of the inner coma. *Astron. Astrophys.* **130**, 361–372.

Crovisier, J. 1998. Physics and chemistry of comets: Recent results from Comets Hyakutake and Hale-Bopp. *Faraday Disc.* **109**, 437–452.

Crovisier, J. 1999. Infrared observations of volatile molecules in Comet Hale-Bopp. *Earth Moon Planets* **79**, 125–143 (1997).

Crovisier, J., and Th. Encrenaz 1983. Infrared fluorescence of molecules in comets: The general synthetic spectrum. *Astron. Astrophys.* **126**, 170–182.

Crovisier, J., K. Leech, D. Bockelée-Morvan, T. Y. Brooke, M. S. Hanner, B. Altieri, H. U. Keller, and E. Lellouch 1997. The spectrum of Comet Hale-Bopp (C/1995 O1) observed with the Infrared Space Observatory at 2.9 astronomical units from the sun. *Science* **275**, 1904–1907.

Dang-Nhu, M., A. S. Pine, A. Fayt, M. De Vleeschouwer, and C. Lambeau 1983. Les intensités dans la pentade ν_{11}, $\nu_2 + \nu_{12}$, $2\nu_{10} + \nu_{12}$, ν_9 et $\nu_3 + \nu_8 + \nu_{10}$ de $^{12}C_2H_4$. *Can. J. Phys.* **61**, 514–521.

Dang-Nhu, M., A. S. Pine, and W. J. Lafferty 1984. Les intensités dans les bandes ν_5, ν_7, et $\nu_8 + \nu_{11}$ de l'éthane $^{12}C_2H_6$. *Can. J. Phys.* **62**, 512–519.

Dello Russo, N., M. A. DiSanti, M. J. Mumma, K. Magee-Sauer, and T. W. Rettig 1998. Carbonyl sulfide in Comets C/1996 B2 (Hyakutake) and C/1995 O1 (Hale-Bopp): Evidence for an extended source in Hale-Bopp. *Icarus* **135**, 377–388.

Dello Russo, N., M. J. Mumma, M. A. DiSanti, K. Magee-Sauer, R. Novak, and T. W. Rettig 1999. Ethane production and release in Comet C/1995 O1 Hale-Bopp. *Bull. Am. Astron. Soc.* **31**, 1098.

Dello Russo, N., M. J. Mumma, M. A. DiSanti, K. Magee-Sauer, R. Novak, and T. W. Rettig 2000. Water production and release in Comet C/1995 O1 Hale-Bopp. *Icarus* **143**, 324–337.

Despois, D., J. Crovisier, D. Bockelée-Morvan, J. Schraml, T. Forveille, and E. Gerard 1986. Observations of hydrogen cyanide in Comet Halley. *Astron. Astrophys.* **160**, L11–12.

DiSanti, M. A., M. J. Mumma, N. Dello Russo, K. Magee-Sauer, R. Novak, and T. W. Rettig 1999. Identification of two sources of carbon monoxide in Comet Hale-Bopp. *Nature* **399**, 662–665.

DiSanti, M. A., M. J. Mumma, N. Dello Russo, and K. Magee-Sauer 2001. Carbon monoxide production and excitation in Comet C/1995 O1 (Hale-Bopp): Isolation of native and distributed CO sources. *Icarus*, in press.

DiSanti, M. A., M. J. Mumma, T. R. Geballe, and J. K. Davies 1995. Systematic observations of methanol and other organics in Comet P/Swift-Tuttle: Discovery of new spectral structure at 3.42 μm. *Icarus* **116**, 1–17.

Eberhardt, P. 1999. Comet Halley's gas composition and extended sources: Results from the neutral mass spectrometer on Giotto. *Space. Sci. Rev.* **90**, 45–52.

Eberhardt, P., D. Krankowsky, W. Schulte, U. Dolder, P. Lämmerzahl, J. J. Berthelier, J. Woweries, U. Stubbemann, R. R. Hodges, J. H. Hoffman, and J. M. Illiano 1987. The CO and N_2 abundance in Comet P/Halley. *Astron. Astrophys.* **187**, 481–484.

Feldman, P. D. 1983. Ultraviolet spectroscopy and the composition of cometary ice. *Science* **219**, 347–354.

Greenberg, J. M., and J. I. Hage 1990. From interstellar dust to comets: A unification of observational constraints. *Astrophys. J.* **361**, 260–274.

Greene, T. P., A. T. Tokunaga, D. W. Toomey, and J. B. Carr 1993. CSHELL: A high spectral resolution 1–5 μm cryogenic echelle spectrograph for the IRTF. *Proc. SPIE* **1946**, 313–324.

Herzberg, G. 1945. *Molecular Spectra and Molecular Structure II: Infrared and Raman Spectra of Polyatomic Molecules.* Van Nostrand Reinhold, New York.

Hiraoka, K., T. Takayama, A. Euchi, H. Handa, and T. Sato 2000. Study of the reactions of H and D atoms with solid C_2H_2, C_2H_4, and C_2H_6 at cryogenic temperatures. *Astrophys. J.* **532**, 1029–1037.

Hoban, S., M. J. Mumma, D. C. Reuter, M. DiSanti, and R. R. Joyce 1991. A tentative identification of methanol as the progenitor of the 3.52-μm emission feature in several comets. *Icarus* **93**, 122–134.

Huebner, W. F., J. J. Keady, and S. P. Lyon 1992. Solar photo rates for planetary atmospheres and atmospheric pollutants. *Astrophys. Space Sci.* **195**, 1–294.

Jessberger, E. K., J. Kissel, H. Fechtig, and F. R. Krueger 1988. Aspects of the major element composition of Halley's dust. *Nature* **332**, 691–695.

Jewitt, D., and H. E. Matthews 1999. Particulate mass loss from Comet Hale-Bopp. *Astron. J.* **117**, 1056–1062.

Kissel, J., and 18 colleagues 1986. Composition of Comet Halley dust particles from Giotto observations. *Nature* **321**, 336–337.

Krasnopolsky, V. A., M. J. Mumma, M. Abbott, B. C. Flynn, K. J. Meech, D. K. Yeomans, P. D. Feldman, and C. B. Cosmovici 1997. Detection of soft X-rays and a sensitive search for noble gases in Comet Hale-Bopp (C/1995 O1). *Science* **277**, 1488–1491.

Kunde, V. G., and J. C. Maguire 1974. Direct integration transmittance model. *J. Quant. Spectrosc. Radiat. Transfer* **14**, 803–817.

Magee-Sauer, K., M. J. Mumma, M. A. DiSanti, N. Dello Russo, and T. W. Rettig 1999. Infrared spectroscopy of the ν_3 band of hydrogen cyanide in C/1995 O1 Hale-Bopp. *Icarus* **142**, 498–508.

Meier, R., T. C. Owen, D. C. Jewitt, H. E. Matthews, N. Biver, D. Bockelée-Morvan, J. Crovisier, and D. Gautier 1998b. Deuterium in Comet C/1995 O1 (Hale-Bopp): Detection of DCN. *Science* **279**, 1707–1710.

Meier, R., T. C. Owen, H. E. Matthews, D. C. Jewitt, D. Bockelée-Morvan, N. Biver, J. Crovisier, and D. Gautier 1998a. A determination of the HDO/H_2O ratio in Comet C/1995 O1 (Hale-Bopp). *Science* **279**, 842–844.

Mélen, F., M. Herman, G. Y. Matti, and D. M. McNaughton 1993. Fourier transform jet spectrum of the ν_7 band of C_2H_6. *J. Mol. Spectrosc.* **160**, 601–603.

Mumma, M. J. 1997. Organic volatiles in comets: Their relation to interstellar ices and solar nebula material. *Astron. Soc. Pac. Conf. Ser.* **122**, 369–396.

Mumma, M. J., and D. C. Reuter 1989. On the identification of formaldehyde in Halley's Comet. *Astrophys. J.* **344**, 940–948.

Mumma, M. J., and 17 colleagues 2001a. A survey of organic volatile species in Comet C/1999 H1 (Lee) using NIRSPEC at the Keck Observatory. *Astrophys. J.* **546**, 1183–1193.

Mumma, M. J., N. Dello Russo, M. A. DiSanti, K. Magee-Sauer, R. E. Novak, S. Brittain, T. Rettig, I. S. McLean, D. C. Reuter, and Li-H. Xu 2001b. Organic composition of C/1999 S4 (LINEAR): A comet formed near Jupiter? *Science* **292**, 1334–1339.

Mumma, M. J., N. Dello Russo, M. A. DiSanti, K. Magee-Sauer, R. Novak, A. Conrad, and F. Chaffee 2001c. *Comet c/1999 T1 (McNaught–Hartley).* IAU Circular 7578.

Mumma, M. J., M. A. DiSanti, N. Dello Russo, M. Fomenkova, K. Magee-Sauer, C. D. Kaminski, and D. X. Xie 1996. Detection of abundant ethane and methane, along with carbon monoxide and water, in Comet C/1996 B2 Hyakutake: Evidence for interstellar origin. *Science* **272**, 1310–1314.

Mumma, M. J., M. A. DiSanti, N. Dello Russo, K. Magee-Sauer, and T. W. Rettig 2000. Detection of CO and ethane in Comet 21P/Giacobini-Zinner: Evidence for variable chemistry in the outer solar nebula. *Astrophys. J.* **531**, L155–L159.

Mumma, M. J., H. A. Weaver, H. P. Larson, D. S. Davis, and M. Williams 1986. Detection of water vapor in Halley's Comet. *Science* **232**, 1523–1528.

Notesco, G., D. Laufer, and A. Bar-Nun 1997. The source of the high C_2H_6/CH_4 ratio in Comet Hyakutake. *Icarus* **125**, 471–473.

Nyquist, I. M., I. M. Mills, W. B. Person, and B. C. Crawford, Jr. 1957. Vibrational intensities. VII. Ethane and ethane-d6. *J. Chem. Phys.* **26**, 552–558.

Pine, A. S., and W. J. Lafferty 1982. Torsional splittings and assignments of the Doppler-limited spectrum of ethane in the C-H stretching region. *J. Res. Natl. Bur. Standard* **87**, 237–256.

Pine, A. S., and S. C. Stone 1996. Torsional tunneling and A_1-A_2 splittings and air broadening of the ${}^{r}Q_0$ and ${}^{p}Q_3$ subbranches of the ν_7 band of ethane. *J. Mol. Spectrosc.* **175**, 21–30.

Reuter, D. C. 1992. The contribution of methanol to the 3.4 micron emission feature in comets. *Astrophys. J.* **386**, 330–335.

Rogers, D. J. 1980. *Infrared Intensities of Alcohols and Ethers.* Ph. D. dissertation, University of Florida.

Rothman, L. S., and 13 colleagues 1992. The HITRAN molecular database: Editions of 1991 and 1992. *J. Quant. Spectrosc. Radiat. Transfer* **48**, 469–507.

Sartakov, B. G., J. Oomens, J. Reuss, and A. Fayt 1997. Interaction of vibrational fundamental and combination states of ethylene in the 3 μm region. *J. Mol. Spectrosc.* **185**, 31–47.

Schloerb, F. P., W. M. Kinzel, D. A. Swade, and W. M. Irvine 1986. HCN production from Comet Halley. *Astrophys. J.* **310**, L55–L60.

Stern, S. A., D. C. Slater, M. C. Festou, J. Wm. Parker, G. R. Gladstone, M. F. A'Hearn, and E. Wilkinson 2000. The discovery of argon in C/1995 O1 (Hale-Bopp). *Astrophys. J.* **544**, L169–L172.

Van Lerberghe, D., I. J. Wright, and J. L. Duncan 1972. High-resolution infrared spectrum and rotational constants of ethylene-H_4. *J. Mol. Spectrosc.* **42**, 251–273.

Weaver, H. A., T. Y. Brooke, G. Chin, S. J. Kim, D. Bockelée-Morvan, and J. K. Davies 1999a. Infrared spectroscopy of Comet Hale-Bopp. *Earth Moon Planets* **78**, 71–80 (1997).

Weaver, H. A., G. Chin, D. Bockelée-Morvan, J. Crovisier, T. Y. Brooke, D. P. Cruikshank, T. R. Geballe, S. J. Kim, and R. Meier 1999c. An infrared investigation of volatiles in Comet 21P/Giacobini-Zinner. *Icarus* **142**, 482–497.

Weaver, H. A., P. D. Feldman, M. F. A'Hearn, C. Arpigny, J. C. Brandt, and S. A. Stern 1999b. Post-perihelion HST observations of Comet Hale-Bopp (C/1995 O1). *Icarus* **141**, 1–12.

Wilson, E. B., Jr. 1938. Nuclear spin and symmetry effects in the heat capacity of ethane gas. *J. Chem. Phys.* **6**, 740–745.

Xie, X., and M. J. Mumma 1996. Monte Carlo simulation of cometary atmospheres: Application to Comet P/Halley at the time of the Giotto spacecraft encounter. II. Axisymmetric model. *Astrophys. J.* **464**, 457–475.